Astronomy & Astrophysics manuscript no. PleiadesLiGK_Barrado
August 10, 2016
©ESO 2016

arXiv:1608.02751v1 [astro-ph.SR] 9 Aug 2016

The seven sisters DANCe

II: Proper motions and the Lithium-Rotation-Activity connection for G and K Pleiads

D. Barrado[1], H. Bouy[1], J. Bouvier[2], E. Moraux[2], L. M. Sarro[3], E. Bertin[4], J.C. Cuillandre[5], J.R. Stauffer[6], J. Lillo-Box[7], and A. Pollock[8]

[1] Depto. Astrofísica, Centro de Astrobiología (INTA-CSIC), ESAC campus, Camino Bajo del Castillo s/n, E-28692 Villanueva de la Cañada, Spain
[2] UJF-Grenoble 1/CNRS-INSU, Institut de Planétologie et d'Astrophysique de Grenoble (IPAG), UMR 5274, Grenoble, F-38041, France
[3] Dpto. de Inteligencia Artificial, ETSI Informática, UNED, Juan del Rosal, 16, E-28040, Madrid, Spain
[4] CEA/IRFU/SAp, Laboratoire AIM Paris-Saclay, CNRS/INSU, Université Paris Diderot, Observatoire de Paris, PSL Research University, F-91191 Gif-sur-Yvette Cedex, France
[5] CEA/IRFU/SAp, Laboratoire AIM Paris-Saclay, CNRS/INSU, Université Paris Diderot, Observatoire de Paris, PSL Research University, F-91191 Gif-sur-Yvette Cedex, France
[6] Spitzer Science Center, California Institute of Technology, Pasadena, CA 91125, USA.
[7] European Southern Observatory, Alonso de Cordova 3107, Vitacura Casilla 19001, Santiago 19, Chile
[8] European Space Agency XMM-Newton Science Operations Centre, European Space Astronomy Centre, P.O. Box 50727, Villafranca del Castillo, E-28080 Madrid, Spain

Received , 2014; accepted

ABSTRACT

Context. Stellar clusters are open windows to understand stellar evolution. Specifically, the change with time and the dependence on mass of different stellar properties. As such, they are our laboratories where different theories can be tested.
Aims. We try to understand the origin of the connection between lithium depletion in F, G and K stars, rotation and activity, in particular in the Pleiades open cluster.
Methods. We have collected all the relevant data in the literature, including information regarding rotation period, binarity and activity, and cross-matched with proper motions, multi-wavelength photometry and membership probability from the DANCe database. In order to avoid biases, only Pleiades single members with probabilities larger than 75% have been included in the discussion.
Results. The analysis confirms that there is a strong link between activity, rotation and the lithium equivalent width excess, specially for the range $Lum(bol) = 0.5 - 0.2\ L_{\odot}$ (about K2-K7 spectral types or 0.75–0.95 $M_{\odot}$).
Conclusions. It is not possible to disentangle these effects but we cannot exclude that the observed lithium overabundance is partially an observational effect due to enhanced activity, due to a large coverage by stellar spots induced by high rotation rates. Since a *bona fide* lithium enhancement is present in young, fast rotators, both activity and rotation should play a role in the lithium problem.

Key words. Stars: pre-main sequence – Stars: formation – Stars: low-mass, brown dwarfs – (Galaxy:) open clusters and associations: individual: The Pleiades

1. Introduction

The Pleiades open cluster does not only offer us a beautiful spectacle during the Fall, it is one of the best studied stellar associations and one of the cornerstones in order to understand stellar properties and evolution. In fact, the literature includes more than one thousand refereed papers dealing with the Pleiades, most of them using the Pleiades as a reference, only in the last ten years. In spite of this, the Pleiades cluster still keeps many secret and basic parameters, such as its distance and age, are not unambiguously established. Even its census is incomplete, although the recent works by Stauffer et al. (2007), Lodieu et al. (2012) and Bouy et al. (2013) have improved considerably the membership list, In fact, Bouy et al. (2015) has increased the number of known members by a 50%, by using public archival data, very accurate proper motions and multi-wavelength photometry (see additional details in Sarro et al. 2014). Regarding its distance, there are currently two different methodologies, based, respectively, on parallaxes from Hipparcos (Perryman et al. 1997) and isochrone fitting. Pre-Hipparcos distances for the Pleiades range between 125 and 130 pc (see, for instance, Soderblom et al. 1993d), whereas the initial distance derived by Hipparcos is much closer, about 119 pc (van Leeuwen 1999). This last value is significantly different to the distance derived by Pinsonneault et al. (1998), who used color-magnitude diagrams and fitting isochrones and obtained 133.5 ± 1.2 pc. More recently, van Leeuwen (2009), by re-analyzing Hipparcos data, has derived a distance of 120.2 ± 1.9 pc. Note that these values should correspond to the distance to the cluster center, whose core radius should be around 3 degrees, which corresponds to 5-6 pc. Another trigonometric parallax, based on HST data and three members, comes from Soderblom et al. (2005), which produced 134.6 ± 3.1 pc. Lately, Melis et al. (2014) have derived

Send offprint requests to: D. Barrado

136.2 ± 1.2 pc based on an accurate parallax for four bona-fide members obtained with the VLBI, which also agrees with the value derived by Galli et al. (2016, in prep), by using accurate proper motions and the convergence point method (137.7 ± 2.5 pc).

On the other hand, the evolution of lithium, either from the cosmological or from the stellar perspective, has received a significant amount of attention since it gives us access to the early universe, the late evolution of stars or their internal structure. In this last case, since its abundance depends on stellar age (Herbig 1965), it has been used as an evolutionary tracker. However, we are far from understanding all sides of the lithium problem.

For FGK members belonging to open clusters there is a clear dependence of the lithium abundance with mass, age and other parameters such as rotation/activity. In fact, standard models predict that the depletion happens during the Pre-Main Sequence evolution. However, the observations show that the depletion continues beyond the arrival to the ZAMS, so additional, non-standard mixing has to take place. Moreover, for clusters older than the Pleiades there is a narrow effective temperature range (6400-6900 K) which shows a large depletion of lithium abundance due to non-standard mixing, the so called lithium gap, dip or chasm (Boesgaard & Tripicco 1986a; Michaud & Charbonneau 1991; Balachandran 1995). In any case, the complexity of the evolution has been established by multiple studies focusing on clusters of different ages. Seminal papers, to name a few, are Pilachowski et al. (1984), Pilachowski (1986), Pilachowski et al. (1987), Pilachowski et al. (1988), Pasquini et al. (1997), Pasquini et al. (2008) for NGC7789, the Pleiades, NGC752, and M67; Boesgaard & Tripicco (1986b), Boesgaard (1987b), Boesgaard (1987a), Boesgaard et al. (1988), Boesgaard & Budge (1988), Boesgaard & Budge (1989), Thorburn et al. (1993), Barrado y Navascues & Stauffer (1996)) for the Hyades, Coma, the Pleiades and Alpha Per, and Praesepe; Soderblom et al. (1993a), Soderblom et al. (1993b), Soderblom et al. (1993c) for Praesepe, the Pleiades and Ursa Majoris moving group. More recently, additional observations for clusters, generally younger, have been studied. Again, just to provide some references: NGC2516 and M35, almost Pleiades twins (Jeffries et al. 1998; Barrado y Navascués et al. 2001a), IC2602 and IC2391 (Barrado y Navascués et al. 1999; Randich 2001; Randich et al. 2001; Barrado y Navascués et al. 2004), NGC2547 (Jeffries et al. 2003), IC4665 (Jeffries et al. 2009), and Collinder 69 (Dolan & Mathieu 1999, Bayo et al. 2012). In the very near future, the large scale spectroscopic survey Gaia-ESO (Gilmore et al. 2012; Randich et al. 2013) will provide an extended database. Recent example is the case of the Vela OB2 association (Sacco et al. 2015).

Lately, several works have been published trying to understand the lithium content in solar-type stars from different perspectives. Bouvier (2008) –see also Eggenberger et al. 2012– investigates the effect of the disk life-time on the rotation and lithium: slow rotation would be the consequence of long-lasting star-disk interaction during the PMS and would produce a significant decoupling between the core and the convective envelope, with the final consequence of extra-mixing and higher lithium depletion. The analysis by Bouvier et al. (2016) of the Gaia-ESO data corresponding to 5 Myr old cluster NGC226 shows a lithium enhancement for fast rotators in with effective temperature in the range 3800-4400 K. On the other hand, Somers & Pinsonneault (2014) argue that the strong magnetic field in fast rotators during the early PMS enlarges the radii and diminishes the temperature of the bottom of the convective envelope, provoking over-abundances. The effective temperature would also be affected, due to the larger spot coverage (with cooler temperatures). These investigations assume that the lithium spread for a given mass corresponds to real abundance differences. However, on the other side, Stuik et al. (1997), Jeffries (1999), King et al. (2000), Barrado y Navascués et al. (2001b), King & Schuler (2004), King et al. (2010), all in the case of the Pleiades but with very different approaches, have tried to verify whether the real cause is related to the presence of surface inhomogeneities and their effect on the observed lithium equivalent width. Some of these works conclude that at least partially the spread is due to atmospheric effects, others argue that most come from real differences in the depletion rate during the PMS evolution. The debate is still open. Here, we reanalyze the complete data-set using the new membership probability and rotation periods, and try to shed new light regarding the lithium depletion in connection with rotation and stellar activity.

2. The data

2.1. Proper motions and photometry from DANCe and TYCHO

The starting point of this analysis is the quasi-complete census of Pleiades members obtained by Bouy et al. (2015), within the DANCe project (Dynamical Analysis of Nearby Clusters, Bouy et al. 2013). The catalog has been produced by essentially retrieving all the public data corresponding to large format detectors in the available open archives, reprocessing and deriving new astrometric solutions, including the correction of distortions due to the diverse instrumentation. The large temporal base-line of this amazing database and the very accurate astrometry have been used to derived very precise proper motions for the initial sample of almost 2,000,000 objects.

Bouy et al. (2013) contains the first release of the DANCe-Pleiades catalogue. The second release is described in details in Bouy et al. (2015). Briefly, the main improvements with respect to the first consists on: the addition of AAVSO Photometric All-Sky Survey DR7 (APASS) *gri* photometry and the analysis of the Tycho-2 catalogue (Høg et al. 2000), since some Pleiades members are too bright for DANCe. The Tycho-2 photometry was complemented with APASS, 2MASS and CMC-14 photometry, and the selection method described in Sarro et al. (2014) was applied to the merged catalogue within the same area as the DANCe-Pleiades survey. A total of 207 high probability, bright members were identified, nicely complementing the DANCe-Pleiades catalog at the bright end of the luminosity function.

Both proper motions and the multi-wavelength photometry have fed a robust method based on statistic probabilities, and we have extracted the probable members, with probabilities larger than 75%. This probability (PrAll, our cut-off for membership) has been derived using the position in several Color-Magnitude diagrams and the proper motions. Details can be found in Sarro et al. (2014). The Pleiades list includes 2109 stellar and substellar members and it has a comprehensive and homogeneous photometry in the Sloan and 2MASS filters.

Note that when there is an overlap between TYCHO and DANCe, we have preferred the TYCHO proper motions (in order to directly compare with previous works) and membership probabilities to DANCe results when plotting the data, when both data-sets were available.

2.2. Lithium from the literature

We have collected all the available data in the literature regarding lithium equivalent width –W(Li)– in members of the Pleiades cluster. Namely, we have searched in the following studies: Soderblom et al. (1993b), Garcia Lopez et al. (1994), Marcy et al. (1994), Basri et al. (1996), Jones et al. (1996), Rebolo et al. (1996), Oppenheimer et al. (1997), Martin et al. (1998), Stauffer et al. (1998a), Jeffries (1999), Martín et al. (2000), Pinfield et al. (2003), Margheim (2007), King et al. (2010), and Dahm (2015). Previous works do not add additional stars to this compilation, and have large uncertainties in their lithium equivalent widths.

In total, our compilation includes 210 objects, reaching around the substellar border-line at 0.072 $M_{\odot}$, and some of them have up to six individual lithium equivalent width measurements, totalling 398 data-points. This collection of 201 stars will be called the Pleiades lithium sample. Note that there is a gap where no observations have been executed between late K and mid-M spectral types. Thus, W(Li) data are not available in the literature since no lithium is expected in this spectral range –T_{eff}=4000-3000 K approximately–, because this element is rapidly exhausted in PMS low-mass stars.

The data are listed in Table 1 –all the lithium equivalent width for the complete data-sample, Table 2 –proper motions and membership probabilities (see subsection 2.3), and Table 3 –ancillary data, including effective temperatures, luminosities, final lithium equivalent widths and abundances and other data (see subsection 3.2 and section 4). Note that for these last two tables we list only the subset corresponding to *bona fide* single stars (additional information in subsection 4.3).

2.3. Additional ancillary data from the literature and the Virtual Observatory

For the sake of completeness, the Pleiades lithium sample also includes additional data from the literature, namely spectral types, rotational periods, and additional photometry in the Johnson and Cousins systems. The photometry comes from the Open Clusters database by Charles Prosser and John Stauffer, a careful compilation of the available data acquired during the XX century. Table 1 from Stauffer et al. (2007) describes the original photometric catalogs, the name prefix used in each of them, the photometric bands and magnitude range for each of them.

We have compiled a secondary sample for completeness and comparison purposes, based on Hertzsprung (1947), Haro et al. (1982), Hambly et al. (1993), and Pinfield et al. (2000), corresponding to Pleiades candidate members with prefix HII, HCG, HHJ and BPL, respectively. After removing the duplications, we have 1131 objects. Then, this sample from the literature was cross-matched with the DANCe and TYCHO catalogs in order to have homogeneous photometry in the Sloan system and membership probabilities (as derived in Sarro et al. 2014). We have retained only those candidate members whose membership probability is larger or equal to 0.75 (as recommended in Sarro et al. 2014), and the sample includes 810 probable Pleiades members. The sample will be called the Pleiades comparison sample.

In addition to the DANCe deep photometry (see subsection 2.1) and the ancillary data from the literature, we have added public photometry using the Virtual Observatory, by taking advantage of the Virtual Observatory Sed Analyzer tool (VOSA, Bayo et al. 2008, Bayo et al. 2016, submitted). VOSA has been designed to perform the following tasks: digests photometric data supplied by the user, searches several photometric catalogs and theoretical models accessible through VO services, fits all the the data to the models, computes the effective temperature and the bolometric luminosity, and provides an estimation of the mass and age of each source. In particular, VOSA explores the WISE (Cutri & et al. 2012), UKIDSS cluster (DR8, Adelman-McCarthy & et al. 2011), GALEX (Bianchi et al. 2011), and 2MASS (Cutri et al. 2003, Skrutskie et al. 2006) archives. In the case of UKIDSS, the data were trimmed by selecting those magnitudes fainter than 13.5 (all $ZYJHK \leq 13.5$mag), in order to avoid non-linearity. Spitzer/IRAC data from Stauffer et al. (2007) have also been added.

3. Membership

3.1. Proper motions and membership probabilities

In Bouy et al. (2013), we presented the DANCe survey of the Pleiades and its new photometric and astrometric catalogue of the cluster reaching an unprecedented accuracy of < 1 mas/yr reaching $i \sim 24.5$ mag, almost 4 mag beyond G=20 mag, the limit provided by the Gaia mission (Prusti et al. 2016, in prep.). Note that for the purposes of this paper, we define a star as a member of the Pleiades if the probability of membership derived in Bouy et al. (2013) is larger than 75%.

Pleiades DANCe proper motions (Bouy et al. 2013) are illustrated in Fig. 1, where we have also included Taurus members based on their proper motions from Ducourant et al. (2005). Note the box framing the vast majority of the Taurus members and the distinct Pleiades population. However, the transition between the loci of both groups is smooth, and some bona-fide Pleiades members lie within the Taurus locus. As a matter of fact, there are several Pleiades candidates with low membership probability (defined as PrAll$\leq$0.75) and detected lithium, some are located far away from the Pleiades median proper motion. This sub-sample will be discussed in 3.3.

A few lithium-rich probable members also have proper motion with significant differences from the average. However, the error-bars are large and all the photometric information suggest that they might be members.

3.2. The Herzprung-Russell diagram

We have taken advantage of VOSA (Bayo et al. 2008, Bayo et al. 2016, submitted) in order to derive basic properties of our samples (the lithium and the comparison samples).

We have derived the bolometric luminosity and effective temperature for each object, by using two sets of theoretical models: Kurucz (Castelli et al. 1997 –any value of $T_{\rm eff}$– and BT-Settl –$T_{\rm eff} \leq 4400$ K– by the Lyon group (Allard et al. 2012). We have restricted our computation to logg=4.5 –valid for the Pleiades age– and solar metallicity. Regarding the distance, we have selected 133 pc (Pinsonneault et al. 1998) with a margin of 5 pc. A different value for the distance (120.2 ± 1.9 pc, van Leeuwen 2009) has been explored and its results will be discussed below. The non-Hipparcos values derived by trigonometric parallaxes by Soderblom et al. (2005) or Melis et al. (2014), –134.6 ± 3.1 or 136.2 ± 1.2 pc, respectively– are essentially the same as the one we have used. The reddening has been fixed at A_v=0.12 mag. Note, however, that there are a dozen of Pleiades members, located South of Merope, that have a larger reddening. In any case, since the reddening vector goes parallel to the MS and these few members do not show any special signature (high or low lithium content, activity), we have not taken this issue into

account. Possible blue excesses were avoided, since neither near UV nor *u* photometry were not included in the fit. Then, we have fitted a third degree polynomial to the best models, minimizing the χ^2. Thus, we derive the optimal $T_{\rm eff}$ and avoid the discrete values returned by VOSA.

Our derived effective temperatures have been compared with values published in the literature and with values derived using colors and there is not obvious differences, although slow rotators (subsection 4.3) tend to have lower $T_{\rm eff}$ when derived with VOSA, and fast rotators show the opposite behavior. In any case, these differences are about 100 K, within the uncertainties of the grid of models used by VOSA.

Regarding the accuracy of the bolometric luminosities derived with VOSA, all objects have enough data-points in their SED to cover at least 25% of the total bolometric flux (i.e., the ratio between the measured fluxes and the derived total flux, and the rest being estimated with the theoretical model). More than 70% of the Pleiades sample with measured lithium has a ratio Flux(measured)/Flux(total) larger than 50%. Thus, we can conclude that both effective temperature and bolometric luminosity are very well characterized. This methodology does not use any estimate from bolometric corrections or a color, which might be strongly biased. Note that individual colors might be affected by different phenomenology, such as activity and variability, and in any case color indices cover a reduced wavelength range and a small fraction of the total luminosity, being subject to a much larger uncertainty than our methodology, which includes all available photometry an a very large range in wavelength coverage.

Our results are displayed in Fig. 2, representing a HR diagram (symbols as in Fig. 1, but in this case only Pleiades data have been included). Two isochrone sets by Siess et al. (2000) and Chabrier et al. (2000) are also displayed. Cluster members follow the 125 Myr isochrone (essentially the ZAMS for the spectral types F, G and K), but the width of the cluster sequence is much larger than the corresponding value due to the binary sequence; and an offset between the data and the Siess et al. (2000) 125 Myr isochrone is relevant. Note that this is also the lithium depletion boundary age of the cluster (Stauffer et al. 1998b). This fact might be related to the distance we have used (133 pc), to the model itself or to the way VOSA fits the effective temperature. However, the proper fitting demands a distance around 115 pc, a value even lower than the Hipparcos estimate. Thus, the feature seems to be real and reveals a problem with the models and/or with the effect of second order parameters such as activity or magnetic fields. Other possible explanation is the known but not completely explained blue excesses for Pleiades members. Stauffer et al. (2003) concludes that the color anomaly –for K members and using color-magnitude diagrams– based on spottiness due to fast rotation and activity. In our sample, the under-luminosity respect the ZAMS also appears for a significant number of F and G stars. As discussed in subsection 4.3, the effect should be the opposite in an HR diagram: activity and the presence of surface inhomogeneities should shift fast rotators towards cooler temperatures (Jackson & Jeffries 2013). Somers & Pinsonneault (2014) (and references there) proposed inflated radii due to rotation and strong magnetic fields. For fainter, cooler members the BT-Settl 120 Myr isochrone describes very well the locus for single members. Somers & Pinsonneault (2015) achieved similar results by focusing on the Pleiades.

One object stands out in the HR diagram: HII2281. It has an anomalous proper motion (Fig. 1 and Hertzsprung 1947) and it should be demoted and rejected as a Pleiades member despite its detected lithium (it was already rejected by Hertzsprung 1947). In any event, this lithium-rich star deserves further study.

3.3. Properties of low-probable members with detected lithium

There are a fair number of Pleiades members (18 without PPL-1), as defined in the literature, with a low probability of being member based on DANCe, and with lithium detection. Most of them have proper motions far away from the cluster median (Fig. 1, magenta solid circles). Some of them have very large errors, but in any case, they seem to be interlopers, in few cases they might belong to a "loose" Taurus population, in similar fashion to what can be found in Orion (Alves & Bouy 2012; Bouy et al. 2014).

As a matter of fact, we can distinguish four different groups among these possible interlopers, depending on the position on the proper motion diagram (Fig. 1) and the errors, and the photometry: The Pleiades candidates with proper motions similar to Taurus and small errors (HII2281, HII0885); a similar group with large error-bars (HII2984, Pels173, Pels112); another with problematic photometry and proper motions compatible with Pleiades membership (HII0248, HII0303, HII0738, HII1275, HII1912, HII2908, HII3197, Pels41 and HCG509); and the few objects with very different movement (HII0697, HCG131, Pels43 and CFHT-PL-15). The first two groups might belong to the the spread Taurus-like population, probably several million years old or to the so called Local Association (the Pleiades super-cluster, Eggen 1975, Eggen 1995), a collection of young stars with similar kinematic properties, which are not necessarily coeval (they might be grouped by gravitational resonances of the galactic potential). This situation (possible relation to the Local Association) might happen for the last group.

Regarding the nine objects with problematic photometry, several might be binary or multiple systems (HII0303, HII0738, HII3197, HCG509), due their position in the HR diagram (Fig. 2). In addition, HCG509 and HII3197 have membership probabilities of 0.16 and 0.71, respectively, and even in the case of HCG509, a Li-rich mid-M (Oppenheimer et al. 1997), non-membership is not assured. The other five stars (HII0248, HII1275, HII1912, HII2908, and Pels41) have membership probability between 0.55 and 0.72 and they should be considered as bona-fide members.

In any case, we can conclude that the 0.75 membership threshold is the one that gives the best compromise between completeness and contamination, but considering the strongly bimodality of the distribution of membership probability (a huge peak at 0% and another around 90%) one can say that p=50% is almost certainly a member, and p=15% is also most certainly a non-member.

4. Lithium in members of the Pleiades

4.1. Building a clean a lithium sample for the Pleiades

In order to revisit the lithium problem, we have created an homogeneous sample (at least as much as possible) of bona-fide Pleiades members. First, we have selected only those with membership probabilities larger than 0.75 (see 3.3). Then, for those with several measured W(Li), we have selected only one value among our complete data set of published W(Li). To do so we have followed two different approaches: the primary –selection A– is based on the spectral resolution, whereas the secondary –selection B– essentially depends on the S/N.

In the first case the rationale responds to the clear separation from the lithium feature at 6707.8 Å of the contaminant iron line at 6707.4 Å–i.e., both can be measured. The prioritization has been: King et al. (2010) –R~60 000 in a 9.2m telescope, Jones et al. (1996) –R~45 000 in a 10m telescope, Oppenheimer et al. (1997) –same as previous, Soderblom et al. (1993b) –R~50 000 in a 3m telescope, Margheim (2007) –R~12 800 in a 3.5m telescope with multiplexing, Jeffries (1999) –R~14 500 in a 2.5m telescope, and Garcia Lopez et al. (1994) –R~10 000 in a 4.2m telescope.

For selection B, where the achieved signal-to-noise ratio is paramount, so we have preferred the data coming from spectra acquired with 10-m class telescopes or 4-m class with large multiplexing (i.e., large exposure times) over conventional instruments (long slit, echelle spectrographs) in 4-m, 3-m or 2-m class telescopes. In this case we have followed the hierarchy: King et al. (2010), Margheim (2007), Jones et al. (1996), Jeffries (1999), Oppenheimer et al. (1997), Garcia Lopez et al. (1994), and Soderblom et al. (1993b). Thus, we have selected the values with the smallest individual errors in W(Li), while preserving some homogeneity in the data-set.

The most significant difference between both selections, due to the sample sizes, correspond to values from Margheim (2007) and Soderblom et al. (1993b). The first work compared both data-sets and derived a systematic difference with a mean value of 12 mÅ, being the most recent, taken at higher S/N and lower spectral resolution, higher. This W(Li) offset does not depend in the specifics value and it is essentially constant for all equivalent widths. Margheim (2007) ascribed this difference to a lower continuum for low S/N spectra, although the net effect of spectra taking at significant resolution is to decrease the measured equivalent width. However, Margheim (2007) supports his conclusion with a comparison between abundances derived with equivalent widths and with spectral synthesis.

Regardless the offsets in the individual sources of lithium equivalent widths, our analysis has been done in parallel with both selections and we have not found any significant difference. All values are listed in Table 3.

4.2. Lithium in FGK members

Figure 3 –top panel– shows the lithium equivalent width versus the effective temperature. We have not plotted the errors in W(Li) for clarity, but they are not large in most of the cases (see Table 3). The large spread for a given temperature is quite obvious, as is the dramatic drop after $T_{\rm eff}$=4400 K and the location of the LDB at 2800 K (the blue and the red sides of the lithium abyss, respectively).

We have derived the lithium abundances, defined as A(Li)=12+log (Li/H), using curves of growth by Soderblom et al. (1993b). For objects with effective temperature cooler than 4000 K (the coolest of the curves from Soderblom et al. 1993b), we have assumed this temperature, and derived an abundance just as a reference. We have avoided the mixing of several sets of curves of growth because, for very low temperatures, they produce very different values (see, for instance, the comparison between Palla et al. 2007 and Pavlenko & Magazzu 1996). In any case, this assumption does not affect our discussion, since most of the object below 4000 K have lithium upper limits and those with actual detections have $T_{\rm eff}\leq$2600 and should have a cosmic, undepleted abundance (i.e., A(Li)=3.1–3.2).

In order to estimate the errors in the abundance, we have taken into account the original errors in W(Li), as taken from the literature, and the estimated errors for the $T_{\rm eff}$ fit by bootstrapping their values inside their uncertainties.

The results have been displayed in Fig. 3 –bottom panel. The diagram also includes the theoretical lithium depletion computed in the BT-Settl models (50, 90, 125, and 150 Myr). As can be seen, the models reproduce very well the location of the LDB, but since they do not include all the complex affects going on for F, G and K stars, they are only indicative for the blue side.

The lithium spread for stars with the same temperature is very evident for any spectral type, but it is even more conspicuous for $T_{\rm eff}$=5200-4000 K. In fact, there is a relation with the bolometric luminosities: the higher the W(Li), the higher the bolometric luminosity and might be related with binarity (see the case of the Hyades, Barrado y Navascues & Stauffer 1996) and/or rotation. This will be examined in greater detail in subsection 4.4.

Some stars with high lithium abundance and $T_{\rm eff}$ around 4500 K have low membership probability. They tend to have larger luminosities and some of them might be pollutants (see subsection 3.3).

The Pleiades members confirmed by DANCe with a G-K spectral type have lithium abundances corresponding, *grosso modo*, to the expected values for their age, even taking into account the lithium spread for the same $T_{\rm eff}$. This fact does not agree with the models of Baraffe & Chabrier (2010), where they predict that episodic accretion events during the PMS could produce ZAMS age GK stars that are severely depleted in lithium (hence calling into question use of lithium as a membership indicator in young clusters like the Pleiades). A similar investigation by Sergison et al. (2013) has not found this effect either.

As stated before, the lithium depletion pattern has received a significant amount of attention both from the theoretical and the observational points of view. Very recently Somers & Pinsonneault (2014) linked the effect of inflated radii due to rotation and strong magnetic fields with lithium depletion. Before, Bouvier (2008) postulated that the basic reason was different disk life-time for fast and slow rotators, the rotation evolution, and the extra lithium mixing due to the shear at the bottom of the convective zone. However, it is not clear that such models can explain the full range in lithium seen in the Pleiades: Eggenberger et al. (2012) developed the disk life-time concept further for a 1 $M_{\odot}$ model and predicted a maximum of 0.25 dex change in abundance, totally insufficient. The lack of depletion for 0.9 $M_{\odot}$ at 5000 K for some Pleiades members, normally fast rotators, is unexplained by any model, and in any case, regarding the results by Somers & Pinsonneault (2014), the lithium-rotation connection cannot be reproduced by their scenario, since essentially all very young PMS stars are in a saturated activity regime, and there is thus no activity (hence radius inflation) – rotation connection (see the case of h Per, Argiroffi et al. 2013).

4.3. Binarity and Rotation: an effect on the HRD location ?

The evolution of the lithium abundance in a star is affected by rotation. Binarity might play a role too. This fact is very relevant in the case of Tidally Locked Binary Systems (with Prot≤15 days), as shown in chromospherically active binaries (Barrado y Navascues et al. 1997), Hyades (Barrado y Navascues & Stauffer 1996) or Praesepe members (King & Hiltgen 1996). Several works have searched for binaries in the Pleiades (Mermilliod et al. 1992; Rosvick et al. 1992; Bouvier et al. 1997b; Queloz et al. 1998) and we have identi-

fied them in our sample. However, some unaccounted for binary and multiple systems might be present too. In order to detect them, we have investigated the position of our sample of G and K Pleiades in an HR diagram. Known visual and spectroscopic binaries have been highlighted with large black circles in Fig. 4. They tend to be brighter than single stars for the same effective temperature, although there is a significant number of bright, "single" stars (indicated as broken large black circle in the diagram). Therefore, we have classified them as "suspected" binaries. The possible relation between rotation and the lithium spread, including binaries, will be investigated in subsection 4.4.

Regarding rotation, we have cross-correlated our data with the rotational periods derived by Hartman et al. (2010), and we have classified our sample of lithium members in fast, moderate and slow rotators based on its distribution for different bolometric luminosities (see Fig. 5) or effective temperatures (the results are essentially the same). Although our criteria are somehow arbitrary (the borderlines between groups, see the discussion by Bouvier et al. 1997a regarding the rotation dichotomy and the link with circumstellar disks), they do not affect the general conclusions. Note, however, that rotational periods are not always accurate. As a matter of fact, the comparison between the values from Hartman et al. (2010) and preliminary estimates from Kepler K2 (Howell et al. 2014) indicates that HII1095 belongs to the slow rotation group.

It is worth noting that known binaries tend to rotate slower than single stars (again from Fig. 5), at least for solar-type stars, where the statistics are more robust. The explanation might be due to the synchronization effect: a fraction of the Pleiades binaries would have orbital periods between 2 and 7 days, forcing the rotation period to be equal to the orbital one, and larger than the corresponding value for single, fast rotators with the same luminosity. Note, however, that there is a bias for finding slowly rotating spectroscopic binaries, since short period binaries can be confused with rapid rotators due to the blending of the lines.

Moreover, the symbol code used on Fig. 4 also includes information regarding rotation. An interesting effect might take place: single stars with fast rotation might be, on average, brighter or cooler than other slower single members. However, the effect is far from proved and a Color-Magnitude Diagram shows that single, fast rotating stars fall on top of the slower ones (Stauffer & Hartmann 1987). Lately, Jackson & Jeffries (2013) and Jackson & Jeffries (2014) have investigated this issue and concluded that active Pre-Main Sequence stars have an expanded radius due to the presence of spots, slowing down the descent along the Hayashi tracks, although they cannot rule out that the strong magnetic fields are inhibiting the convective flux transport. Somers & Pinsonneault (2014) predicts larger radius (and cooler temperatures) for fast rotators. A different evolutionary history for fast rotators should have an effect on the lithium content, which would be maintained over the whole stellar timespan. However, the spread for single Hyades stars at about 600 Myr is much smaller than the observed range for the Pleiades. If the effect is real, our interpretation is that the fast rotators appear cooler due to activity, and the overall bolometric luminosity, a quantity that depends on the nuclear reaction in the stellar core, remains essentially unaffected. A significant fraction of their surface should be covered with solar-like spots, with lower temperature, and the Spectral Energy Distribution should be affected by the presence of the spot, shifting the distribution to the red and keeping the total energy output. Note that in order to compute $Lum(bol)$ or $T_{\rm eff}$ we do not rely on bolometric corrections and colors, which can be affected by activity and the presence of surface inhomogeneities. However, we cannot completely discard the other effect discussed above or changes on the stellar structure due to rotation and the centrifugal forces. Color effects due to rotation and activity will be studied in depth somewhere else.

4.4. The lithium spread for G and K stars: rotation versus activity

The lithium spread, specially for K stars, has been discussed by Soderblom et al. (1993b), and extensively examined in the literature for the Pleiades (Garcia Lopez et al. 1994, Jones et al. 1996, Oppenheimer et al. 1997, Jeffries 1999, and King et al. 2010) and for other clusters such as NGC2451 (Hünsch et al. 2004). For more details, see the introduction.

That lithium equivalent widths for young stars are enhanced for rapidly rotating and active K dwarfs is well established, but there is still no universally accepted physical explanation nor agreement as to whether the observed effect is due to differences in lithium abundance or instead is a consequence of differing line formation processes. We have already discussed its relation with activity via surface inhomogeneities in Barrado y Navascués et al. (2001b), and compared with other lines produced by alkali elements such as sodium and potassium, which are not depleted in the stellar interior, concluding that at least *partially* the change in effective temperature (lower when compared with the spotless photosphere) should produce an increase in the observed lithium equivalent width for the same abundance. A similar conclusion has been derived by Randich (2001), at least for stars warmer than $\sim$ 5400 K: activity modifies the potassium equivalent widths, and thus the inferred potassium abundances (but see also the study of stars in the Alpha Per cluster by Martín et al. 2005).

Figure 6 displays our selected values of lithium equivalent width versus the bolometric luminosity (in order to avoid the possible effect by the activity/spotness on the effective temperature). The top panel includes single, known and suspected binaries, whereas, for the sake of simplicity, the bottom panel only displays single stars. Colors and symbols differentiate the three classes of rotators (see Fig. 5). The data for single stars appear in Table 2 and Table 3. The relation between the equivalent width and the rotation for single stars, for the same luminosity, is quite striking, specially for $Lum(bol) = 0.5 - 0.2\ L_{\odot}$ (about K2-K7 spectral types or 0.75–0.95 $M_{\odot}$), but even reaching 1.0 $L_{\odot}$ (about G5 or 1.1 $M_{\odot}$). Stars with very large lithium equivalent width are marked with big open diamonds and will be discussed in some detail. In the case of binaries, fast rotating systems (or suspected binaries) have much larger equivalent widths than slow rotators. Is this a consequence of rotation per se? Note that HII3096 and HII380, the first one having intermediate rotation rate and the last being a slow rotator, have lithium equivalent widths larger than the corresponding value for similar stars. In order to explain these anomalies, lets have a look at the activity effect on W(Li) via surface inhomogeneities.

Figure 7a shows the relation between the photometric variability (the amplitude of the light curve) and the rotational period. As expected, slow rotators have a reduced variability. On the contrary, fast rotators display a large range for the photometric amplitude. There are two explanations for this: either the spots might be distributed very evenly on the stellar surface, or the inclination angle is large (near pole-on), so a stellarspot or a group of them are visible during a significant fraction of the period. Therefore, even if the spot filling factor is large, the photometric variability should be small. In fact, this is what seems to be happening for HII1756 –fast rotator– and HII1593 –slow rotator, as shown in Fig. 7b, where we display the *vsini* versus

the rotational period. In any case, some might have genuine low activity (perhaps reassembling a solar minimum or even a Maunder minimum). Several Pleiades members have been labeled in the diagram. All four slow and moderate rotator with large variability have large W(Li).

What about other signposts of activity? We have compared the X-ray emission (the ratio between the X-ray and the bolometric luminosities) with the rotational periods (Fig. 7c). As expected, the large majority of fast rotators (short *Prot*) have Lum L_X/L_{Bol} near the saturation at a ratio close to −3. Most of these Pleiades members display, indeed, a lithium excess, even if the *Prot* is not remarkably short. In any case, the figures show a trend, no a clear-cut relationship.

In any event, just to verify whether the stellar mass might play a hidden role in the trends discussed above, Fig. 8a compares the ratio Lum L_X/L_{Bol} with the bolometric luminosity (as a proxy of the stellar mass). Clearly, the lithium excesses are related with X-ray overluminosities: the connection rotation-activity-lithium is striking, specially for the luminosity range 0.1-1 $L_\odot$ (up to 1.1 $M_\odot$ or G5 spectral type). Note, however, that the X-ray is coming from the corona and the lithium feature is formed at the photosphere. Thus, the optical variability should be a better indicator of the effect of activity on the observed lithium equivalent width. Therefore, as a cross-check, we have used the amplitude of the light-curve and compared with the bolometric luminosity (Fig. 8b), which support our interpretation.

Thus, although there is no one-to-one relation between lithium over-abundance and rotation and/or activity, we conclude that part of the origin of the observed lithium spread could be activity via surface inhomogeneities. This effect is partially hidden by other factors such as spot filling factor, the inclination of the rotation, and binarity, but the trend is significant. Note, however, that a much younger association, namely NGC2264 displays a clear connection between rotation and lithium which should be intrinsic and cannot be connected to activity, since this 5 Myr sample is saturated (see details in Bouvier et al. 2016). Thus, both factors should be playing a role although the relative importance of these two effects could change at different ages.

4.5. The lithium-chronology: lithium depletion pattern for slow and fast rotators

In order to derive an age estimate for single stars or a new moving group, it is quite common to compare their lithium equivalent widths with the lithium depletion pattern for several well known open clusters and stellar associations at different evolutionary states. However, for a given mass/$T_{\rm eff}$/luminosity, the visual inspection indicates that there is a large spread in W(Li), and there are not clear boundaries between clusters of very different ages.

Since we have clearly established the relation between W(Li) and rotation, independently of the original reason, we propose to make this type of comparison (the lithium-chronology for G and K stars) taking into account the rotation class. A slow rotator should be compared solely with cluster members with large rotational periods and the same holds for fast rotators. Age estimates derived this way should have much smaller error bars.

4.6. Pre-Main Sequence evolution: lithium, rotation, radii and planetary systems

There is a trend between planet host and lithium depletion for solar-like stars (Israelian et al. 2009), in the sense that stars with known planets are, on average, lithium-poor compared with similar stars. Note, however, that it has not been proved that the relation is physical and much work has to be done. If real, the origin of this trend is not understood. On the other hand, there are evidences of planets being engulfed or very close to it (Lillo-Box et al. 2014b, Lillo-Box et al. 2014a) by their host star, leaving abundance abnormalities (Israelian et al. 2001), but they would be enriched by metallic elements. If the trend is real, our interpretation is not related with contamination, but with the early evolution and the connection between the circumstellar disk and rotation (and activity). Weak-line TTauri stars (i.e., diskless) rotate faster than Classical TTauri stars (with circumstellar disk), due to the disk-locking produced by magnetic fields. The dichotomy for the rotation rates are kept as stars evolved towards the Main Sequence (Bouvier et al. 1997a). Once there, the slow rotators have a tendency to have debris disk, the assumed remnant of planet formation, suggesting that they do have a planetary system (Bouvier 2008; McQuillan et al. 2013b, McQuillan et al. 2013a). As we have seen, Pleiades members, already very near the ZAMS, display a clear correlation between rotation and lithium equivalent width. The cause can be either and early effect, intrinsic effect due to rotation (as in the case of NGC2264, Bouvier et al. 2016); and inflated radii due to fast rotation producing a reduced lithium depletion (as postulated by Somers & Pinsonneault 2014, implying a different evolutionary history); or an apparent effect due to the rotation-activity connection, a cooler effective temperature and enhanced lithium equivalent width, without modifying the lithium abundance depletion pattern. Independently of the validity of these three scenarios (perhaps all are at work), the distribution of rotational periods and lithium in Pleiades bona-fide members suggest that the likelihood of finding planetary systems in slow rotators, with lower W(Li), may be much larger than in the case of lithium-rich, fast rotators. Moreover, since the *vsini* and the activity are small, from the technical point of view it would be easier to find them.

5. Conclusions

We have compiled all the available lithium equivalent with in members of the Pleiades open cluster and reassessed the membership probability based on the DANCe database (Sarro et al. 2014; Bouy et al. 2015). In addition, we have compiled multi-wavelength photometry from DANCe and from the literature based on the Virtual Observatory using capabilities of VOSA (Bayo et al. 2008), in order to derive accurate bolometric luminosities and effective temperatures. In addition, we have gathered all the available information regarding rotational periods, projected equatorial velocities, binarity and activity. Thus, we selected a sub-sample of Pleiades members based on their position on the Herzprung-Russell diagram and the membership probability as derived from proper motions and different photometric Color-Magnitude Diagrams.

We have not found any undisputed trend between a star location in the HR diagram and the rotation. If there is, it might be connected with activity and the presence of large coverage by stellar spots, which should affect the derived effective temperature and/or the bolometric luminosity. However, the relation between lithium equivalent with and rotation is much more evident, specially for single stars with the same luminosity in the range $Lum(bol) = 0.5 - 0.2\ L_\odot$ (about K2-K7 spectral types or 0.75–0.95 $M_\odot$), but even reaching 1.0 $L_\odot$ (about G5 or 1.1 $M_\odot$). This lithium excess, which is connected to rotation (Butler et al. 1987; Soderblom et al. 1993b), also seems to be connected with activity (initially suggested by García López et al. 1991), either

in terms of photospheric variability (the amplitude) and X-ray emission (coming from the stellar corona). Thus, although we cannot find a bijective relation either between lithium excess and rotation or activity (in the sense that star with lithium excess are *always* very active and rotate fast and *vice versa*), it seems that part of the explanation falls on the last factor: surface inhomogeneities would modify the observed lithium equivalent. Moreover, since a *bona fide* lithium enhancement is present in young, fast rotators (as the case of NGC2264 illustrates), both activity and rotation should play a role in the lithium problem. In addition, we suggest that, due to the bi- or multi-modal distribution of the rotational periods for a given mass, the gyro-chronology should take this fact into account.

Finally, it is possible to speculate that, **if** there is a connection between lithium and the presence of planets in field stars, Pleiades members with low lithium and slow rotation might have a larger probability of harboring planetary systems.

In any case, since the lithium surface abundance is a probe to the stellar interior and despite quite sophisticated recent theoretical efforts we do not understand its evolution, it seems necessary to revisit the problem with new, homogeneous data taken with a large spectral resolution instrument at a very high signal to noise ratio, coupled with a complete data-set (rotation, activity, other alkali and so on). Thus, only by having all this information at hand we can expected to be able to provide a comprehensive interpretation and the problem be solved.

Acknowledgements. This research has been funded by Spanish grant ESP2015-65712-C5-1-R, as well as by the French grant ANR-10-JCJC-0501 DESC, as well as by the CNRS PICS project “Comprendre l’origine et les proprietes des etoiles jeunes”. HB is funded by the Spanish Ramón y Cajal fellowship program number RYC-2009-04497, whereas JB and EM acknowledge financial support from the grant ANR 2011 Blanc SIMI5-6 020 01 “Toupies: Towards understanding the spin evolution of stars”. We also acknowledge support from the Faculty of the European Space Astronomy Centre (ESAC). It makes use of VOSA, developed under the Spanish Virtual Observatory project supported from the Spanish MICINN through grant AyA2008-02156, and of the SIMBAD database, operated at CDS, Strasbourg, France. This work is based in part on data obtained as part of the UKIRT Infrared Deep Sky Survey; from the Wide-Field Infrared Survey Explorer, which is a joint project of the University of California, Los Angeles, and the Jet Propulsion Laboratory/California Institute of Technology, funded by the National Aeronautics and Space Administration; and data from the Two Micron All Sky Survey, which is a joint project of the University of Massachusetts and the Infrared Processing and Analysis Center/California Institute of Technology, funded by the National Aeronautics and Space Administration and the National Science Foundation. We do greatly appreciate the comments and suggestions bt the anonymous referee.

References

Adelman-McCarthy, J. K. & et al. 2011, VizieR Online Data Catalog, 2306, 0
Allard, F., Homeier, D., Freytag, B., & Sharp, C. M. 2012, in EAS Publications Series, Vol. 57, EAS Publications Series, ed. C. Reylé, C. Charbonnel, & M. Schultheis, 3–43
Alves, J. & Bouy, H. 2012, A&A, 547, A97
Argiroffi, C., Caramazza, M., Micela, G., Moraux, E., & Bouvier, J. 2013, Protostars and Planets VI, 89
Balachandran, S. 1995, ApJ, 446, 203
Baraffe, I. & Chabrier, G. 2010, A&A, 521, A44
Barrado y Navascués, D., Deliyannis, C. P., & Stauffer, J. R. 2001a, ApJ, 549, 452
Barrado y Navascues, D., Fernandez-Figueroa, M. J., Garcia Lopez, R. J., de Castro, E., & Cornide, M. 1997, A&A, 326, 780
Barrado y Navascués, D., García López, R. J., Severino, G., & Gomez, M. T. 2001b, A&A, 371, 652
Barrado y Navascues, D. & Stauffer, J. R. 1996, A&A, 310, 879
Barrado y Navascués, D., Stauffer, J. R., & Jayawardhana, R. 2004, ApJ, 614, 386
Barrado y Navascués, D., Stauffer, J. R., & Patten, B. M. 1999, ApJ, 522, L53
Basri, G., Marcy, G. W., & Graham, J. R. 1996, ApJ, 458, 600
Bayo, A., Barrado, D., Huélamo, N., et al. 2012, A&A, 547, A80
Bayo, A., Rodrigo, C., Barrado y Navascués, D., et al. 2008, A&A, 492, 277
Bianchi, L., Herald, J., Efremova, B., et al. 2011, Ap&SS, 335, 161
Boesgaard, A. M. 1987a, PASP, 99, 1067
Boesgaard, A. M. 1987b, ApJ, 321, 967
Boesgaard, A. M. & Budge, K. G. 1988, ApJ, 332, 410
Boesgaard, A. M. & Budge, K. G. 1989, ApJ, 338, 875
Boesgaard, A. M., Budge, K. G., & Ramsay, M. E. 1988, ApJ, 327, 389
Boesgaard, A. M. & Tripicco, M. J. 1986a, ApJ, 303, 724
Boesgaard, A. M. & Tripicco, M. J. 1986b, ApJ, 302, L49
Bouvier, J. 2008, A&A, 489, L53
Bouvier, J., Forestini, M., & Allain, S. 1997a, A&A, 326, 1023
Bouvier, J., Lanzafame, A. C., Venuti, L., et al. 2016, A&A, 590, A78
Bouvier, J., Rigaut, F., & Nadeau, D. 1997b, A&A, 323, 139
Bouy, H., Alves, J., Bertin, E., Sarro, L. M., & Barrado, D. 2014, A&A, 564, A29
Bouy, H., Bertin, E., Moraux, E., et al. 2013, A&A, 554, A101
Bouy, H., Bertin, E., Sarro, L. M., et al. 2015, A&A, 577, A148
Butler, R. P., Marcy, G. W., Cohen, R. D., & Duncan, D. K. 1987, ApJ, 319, L19
Castelli, F., Gratton, R. G., & Kurucz, R. L. 1997, A&A, 318, 841
Chabrier, G., Baraffe, I., Allard, F., & Hauschildt, P. 2000, ApJ, 542, 464
Cutri, R. M. & et al. 2012, VizieR Online Data Catalog, 2311, 0
Cutri, R. M., Skrutskie, M. F., van Dyk, S., et al. 2003, 2MASS All Sky Catalog of point sources. (The IRSA 2MASS All-Sky Point Source Catalog, NASA/IPAC Infrared Science Archive. http://irsa.ipac.caltech.edu/applications/Gator/)
Dahm, S. E. 2015, ApJ, 813, 108
Dolan, C. J. & Mathieu, R. D. 1999, AJ, 118, 2409
Ducourant, C., Teixeira, R., Périé, J. P., et al. 2005, A&A, 438, 769
Eggen, O. J. 1975, PASP, 87, 37
Eggen, O. J. 1995, AJ, 110, 1749
Eggenberger, P., Haemmerlé, L., Meynet, G., & Maeder, A. 2012, A&A, 539, A70
García López, R. J., Rebolo, R., Beckman, J. E., & Magazzù, A. 1991, in Lecture Notes in Physics, Berlin Springer Verlag, Vol. 380, IAU Colloq. 130: The Sun and Cool Stars. Activity, Magnetism, Dynamos, ed. I. Tuominen, D. Moss, & G. Rüdiger, 443
Garcia Lopez, R. J., Rebolo, R., & Martin, E. L. 1994, A&A, 282, 518
Gilmore, G., Randich, S., Asplund, M., et al. 2012, The Messenger, 147, 25
Hambly, N. C., Hawkins, M. R. S., & Jameson, R. F. 1993, A&AS, 100, 607
Haro, G., Chavira, E., & Gonzalez, G. 1982, Boletin del Instituto de Tonantzintla, 3, 3
Hartman, J. D., Bakos, G. Á., Kovács, G., & Noyes, R. W. 2010, MNRAS, 408, 475
Herbig, G. H. 1965, ApJ, 141, 588
Hertzsprung, E. 1947, Annalen van de Sterrewacht te Leiden, 19, A1
Høg, E., Fabricius, C., Makarov, V. V., et al. 2000, A&A, 355, L27
Howell, S. B., Sobeck, C., Haas, M., et al. 2014, PASP, 126, 398
Hünsch, M., Randich, S., Hempel, M., Weidner, C., & Schmitt, J. H. M. M. 2004, A&A, 418, 539
Israelian, G., Delgado Mena, E., Santos, N. C., et al. 2009, Nature, 462, 189
Israelian, G., Santos, N. C., Mayor, M., & Rebolo, R. 2001, Nature, 411, 163
Jackson, R. J. & Jeffries, R. D. 2013, MNRAS, 431, 1883
Jackson, R. J. & Jeffries, R. D. 2014, MNRAS, 441, 2111
Jeffries, R. D. 1999, MNRAS, 309, 189
Jeffries, R. D., Jackson, R. J., James, D. J., & Cargile, P. A. 2009, MNRAS, 400, 317
Jeffries, R. D., James, D. J., & Thurston, M. R. 1998, MNRAS, 300, 550
Jeffries, R. D., Oliveira, J. M., Barrado y Navascués, D., & Stauffer, J. R. 2003, MNRAS, 343, 1271
Jones, B. F., Fischer, D. A., & Stauffer, J. R. 1996, AJ, 112, 1562
King, J. R. & Hiltgen, D. R. 1996, PASP, 108, 246
King, J. R., Krishnamurthi, A., & Pinsonneault, M. H. 2000, AJ, 119, 859
King, J. R. & Schuler, S. C. 2004, AJ, 128, 2898
King, J. R., Schuler, S. C., Hobbs, L. M., & Pinsonneault, M. H. 2010, ApJ, 710, 1610
Lillo-Box, J., Barrado, D., Henning, T., et al. 2014a, A&A, 568, L1
Lillo-Box, J., Barrado, D., Moya, A., et al. 2014b, A&A, 562, A109
Lodieu, N., Deacon, N. R., & Hambly, N. C. 2012, MNRAS, 422, 1495
Marcy, G. W., Basri, G., & Graham, J. R. 1994, ApJ, 428, L57
Margheim, S. J. 2007, PhD thesis, Indiana University
Martin, E. L., Basri, G., Gallegos, J. E., et al. 1998, ApJ, 499, L61
Martín, E. L., Brandner, W., Bouvier, J., et al. 2000, ApJ, 543, 299
Martín, E. L., Magazzù, A., García López, R. J., Randich, S., & Barrado y Navascués, D. 2005, A&A, 429, 1051
McQuillan, A., Aigrain, S., & Mazeh, T. 2013a, MNRAS, 432, 1203
McQuillan, A., Mazeh, T., & Aigrain, S. 2013b, ApJ, 775, L11
Melis, C., Reid, M. J., Mioduszewski, A. J., Stauffer, J. R., & Bower, G. C. 2014, Science, 345, 1029
Mermilliod, J.-C., Rosvick, J. M., Duquennoy, A., & Mayor, M. 1992, A&A, 265, 513

Michaud, G. & Charbonneau, P. 1991, Space Sci. Rev., 57, 1
Oppenheimer, B. R., Basri, G., Nakajima, T., & Kulkarni, S. R. 1997, AJ, 113, 296
Palla, F., Randich, S., Pavlenko, Y. V., Flaccomio, E., & Pallavicini, R. 2007, ApJ, 659, L41
Pasquini, L., Biazzo, K., Bonifacio, P., Randich, S., & Bedin, L. R. 2008, A&A, 489, 677
Pasquini, L., Randich, S., & Pallavicini, R. 1997, A&A, 325, 535
Pavlenko, Y. V. & Magazzu, A. 1996, A&A, 311, 961
Perryman, M. A. C., Lindegren, L., Kovalevsky, J., et al. 1997, A&A, 323, L49
Pilachowski, C. 1986, ApJ, 300, 289
Pilachowski, C., Saha, A., & Hobbs, L. M. 1988, PASP, 100, 474
Pilachowski, C. A., Booth, J., & Hobbs, L. M. 1987, PASP, 99, 1288
Pilachowski, C. A., Mould, J. R., & Siegel, M. J. 1984, ApJ, 282, L17
Pinfield, D. J., Dobbie, P. D., Jameson, R. F., et al. 2003, MNRAS, 342, 1241
Pinfield, D. J., Hodgkin, S. T., Jameson, R. F., et al. 2000, MNRAS, 313, 347
Pinsonneault, M. H., Stauffer, J., Soderblom, D. R., King, J. R., & Hanson, R. B. 1998, ApJ, 504, 170
Queloz, D., Allain, S., Mermilliod, J.-C., Bouvier, J., & Mayor, M. 1998, A&A, 335, 183
Randich, S. 2001, A&A, 377, 512
Randich, S., Gilmore, G., & Gaia-ESO Consortium. 2013, The Messenger, 154, 47
Randich, S., Pallavicini, R., Meola, G., Stauffer, J. R., & Balachandran, S. C. 2001, A&A, 372, 862
Rebolo, R., Martin, E. L., Basri, G., Marcy, G. W., & Zapatero-Osorio, M. R. 1996, ApJ, 469, L53
Rosvick, J. M., Mermilliod, J.-C., & Mayor, M. 1992, A&A, 255, 130
Sacco, G. G., Jeffries, R. D., Randich, S., et al. 2015, A&A, 574, L7
Sarro, L. M., Bouy, H., Berihuete, A., et al. 2014, A&A, 563, A45
Sergison, D. J., Mayne, N. J., Naylor, T., Jeffries, R. D., & Bell, C. P. M. 2013, MNRAS, 434, 966
Siess, L., Dufour, E., & Forestini, M. 2000, A&A, 358, 593
Skrutskie, M. F., Cutri, R. M., Stiening, R., et al. 2006, AJ, 131, 1163
Soderblom, D. R., Fedele, S. B., Jones, B. F., Stauffer, J. R., & Prosser, C. F. 1993a, AJ, 106, 1080
Soderblom, D. R., Jones, B. F., Balachandran, S., et al. 1993b, AJ, 106, 1059
Soderblom, D. R., Nelan, E., Benedict, G. F., et al. 2005, AJ, 129, 1616
Soderblom, D. R., Pilachowski, C. A., Fedele, S. B., & Jones, B. F. 1993c, AJ, 105, 2299
Soderblom, D. R., Stauffer, J. R., Hudon, J. D., & Jones, B. F. 1993d, ApJS, 85, 315
Somers, G. & Pinsonneault, M. H. 2014, ApJ, 790, 72
Somers, G. & Pinsonneault, M. H. 2015, MNRAS, 449, 4131
Stauffer, J. R. & Hartmann, L. W. 1987, ApJ, 318, 337
Stauffer, J. R., Hartmann, L. W., Fazio, G. G., et al. 2007, ApJS, 172, 663
Stauffer, J. R., Jones, B. F., Backman, D., et al. 2003, AJ, 126, 833
Stauffer, J. R., Schild, R., Barrado y Navascues, D., et al. 1998a, ApJ, 504, 805
Stauffer, J. R., Schultz, G., & Kirkpatrick, J. D. 1998b, ApJ, 499, L199+
Stuik, R., Bruls, J. H. M. J., & Rutten, R. J. 1997, A&A, 322, 911
Terndrup, D. M., Stauffer, J. R., Pinsonneault, M. H., et al. 2000, AJ, 119, 1303
Thorburn, J. A., Hobbs, L. M., Deliyannis, C. P., & Pinsonneault, M. H. 1993, ApJ, 415, 150
van Leeuwen, F. 1999, A&A, 341, L71
van Leeuwen, F. 2009, A&A, 500, 505

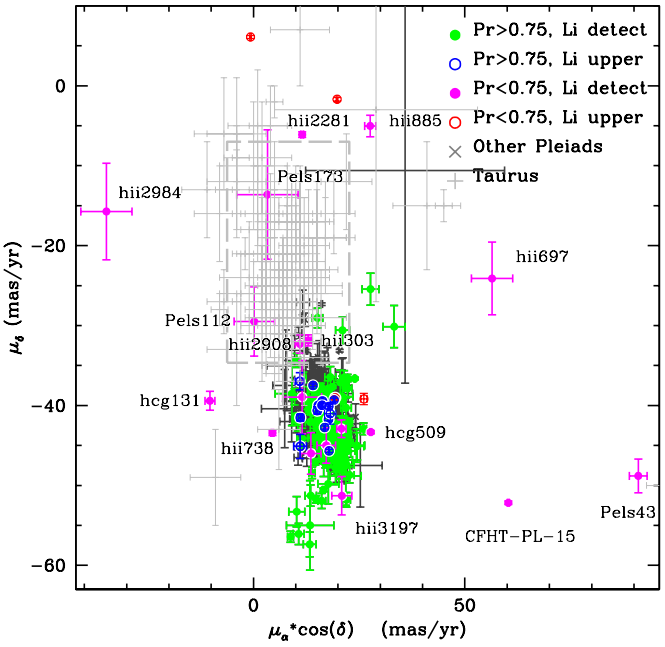

Fig. 1. Proper motions for Pleiades and Taurus-Auriga members. We have distinguished four cases: green solid circles for lithium detection and membership probability larger than 0.75; blue open circles for lithium upper limits and membership probability larger than 0.75; magenta solid circles for lithium detection and membership probability less than 0.75; red open circles for lithium upper limits and membership probability less than 0.75. Membership probabilities come from Bouy et al. (2014). Light grey plus symbols are used for Taurus-Auriga members (taken from Ducourant et al. 2005).

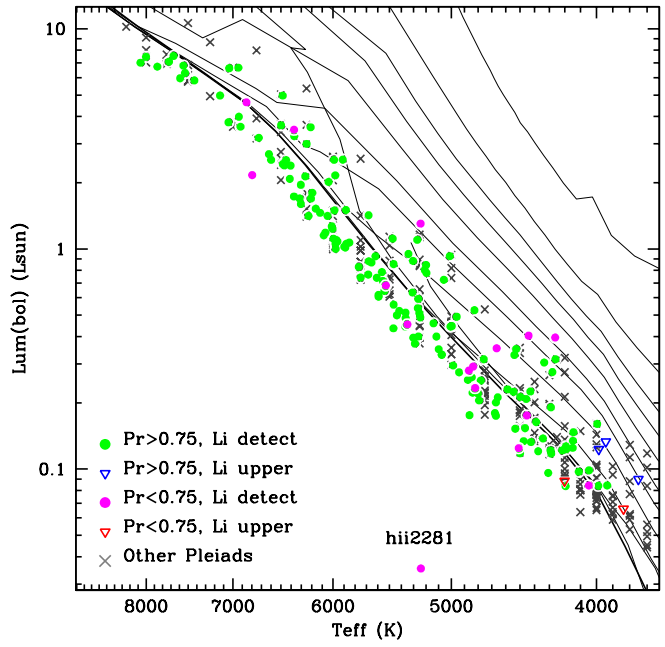

Fig. 2. Hertzsprung-Russell diagrams displaying Pleiades data. The isochrones correspond to Siess et al. (2000) –1, 3, 5, 7, 10, 15, 20, 30, 50, 125, Myr and 5 Gyr– and BT-Settl by the Lyon group (Allard et al. 2012) –1, 20, 120 Myr and 10 Gyr–. The 120/125 Myr isochrones are high-lighted. Symbols as in Fig. 1 .

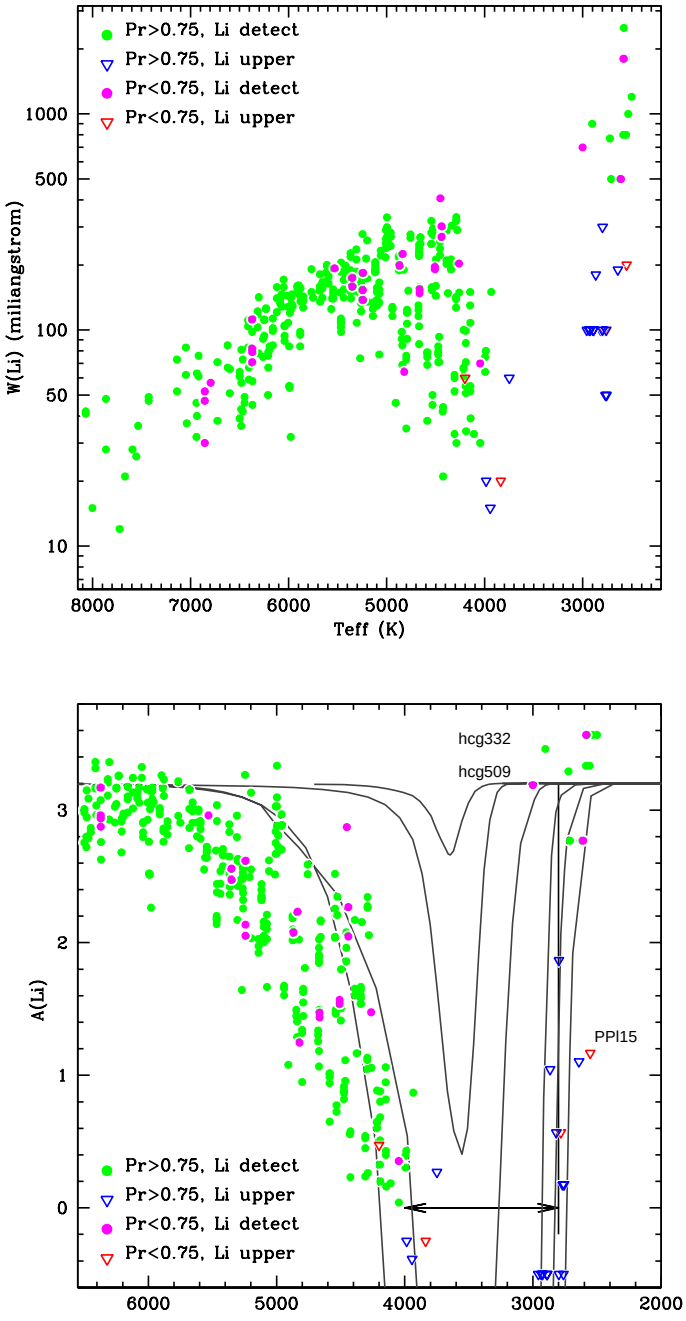

Fig. 3. Lithium equivalent width (top) and lithium abundance (bottom) versus effective temperature. The diagram shows all relevant data, including multiple measurements for the same stars and known binaries. Symbols correspond to: green solid circles are used for lithium detection and membership probability larger than 0.75 (from Bouy et al. 2014); blue open triangles for lithium upper limits and membership probability larger than 0.75; magenta solid circles for lithium detection and membership probability less than 0.75; red open triangles for lithium upper limits and membership probability less than 0.75. Membership probabilities come from (from Bouy et al. 2014). The curves correspond to BT-Settl models from Allard et al. (2012). The central dips are for 10 and 20 Myr, the blue side of the lithium abyss includes values for 50 and 125 Myr, and the red side displays the computation for 50, 90, 125 and 150 Myr.

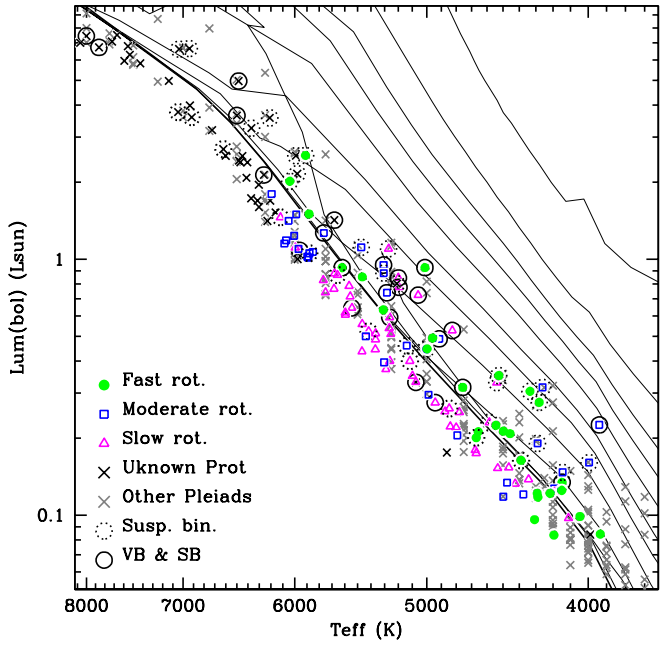

Fig. 4. Zoom for the Hertzsprung-Russell diagram displaying Pleiades FGK members. The isochrones correspond to Siess et al. (2000), with ages of 1, 3, 5, 7, 10, 15, 20, 30, 50, 125, Myr and 5 Gyr. The 125 Myr isochrone is high-lighted. Fast (green solid circles), moderate (open blue squares) and slow (open magenta triangles) rotators are defined by their location within the period vs. luminosity plot shown in Fig. 5. The same symbol and color code are used in the and following figures. Empty large black circles for binaries (broken lines for suspected binaries).

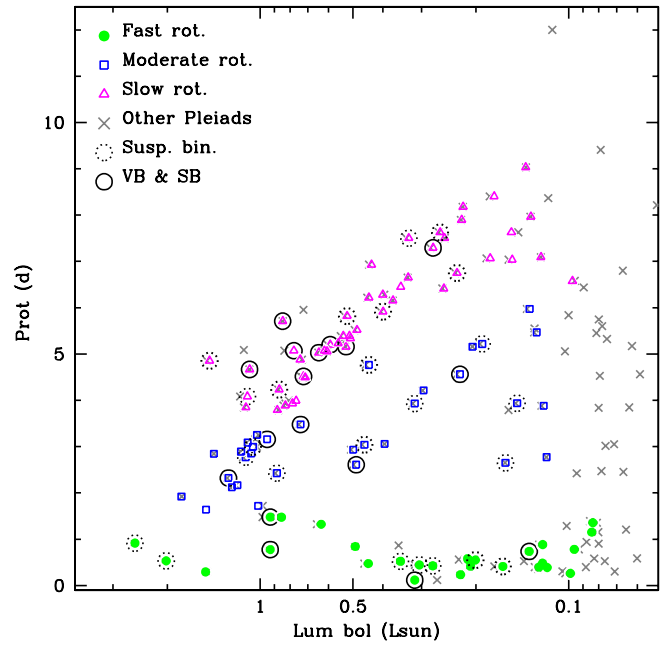

Fig. 5. Rotation period versus the bolometric luminosity. Symbols as in Fig. 4.

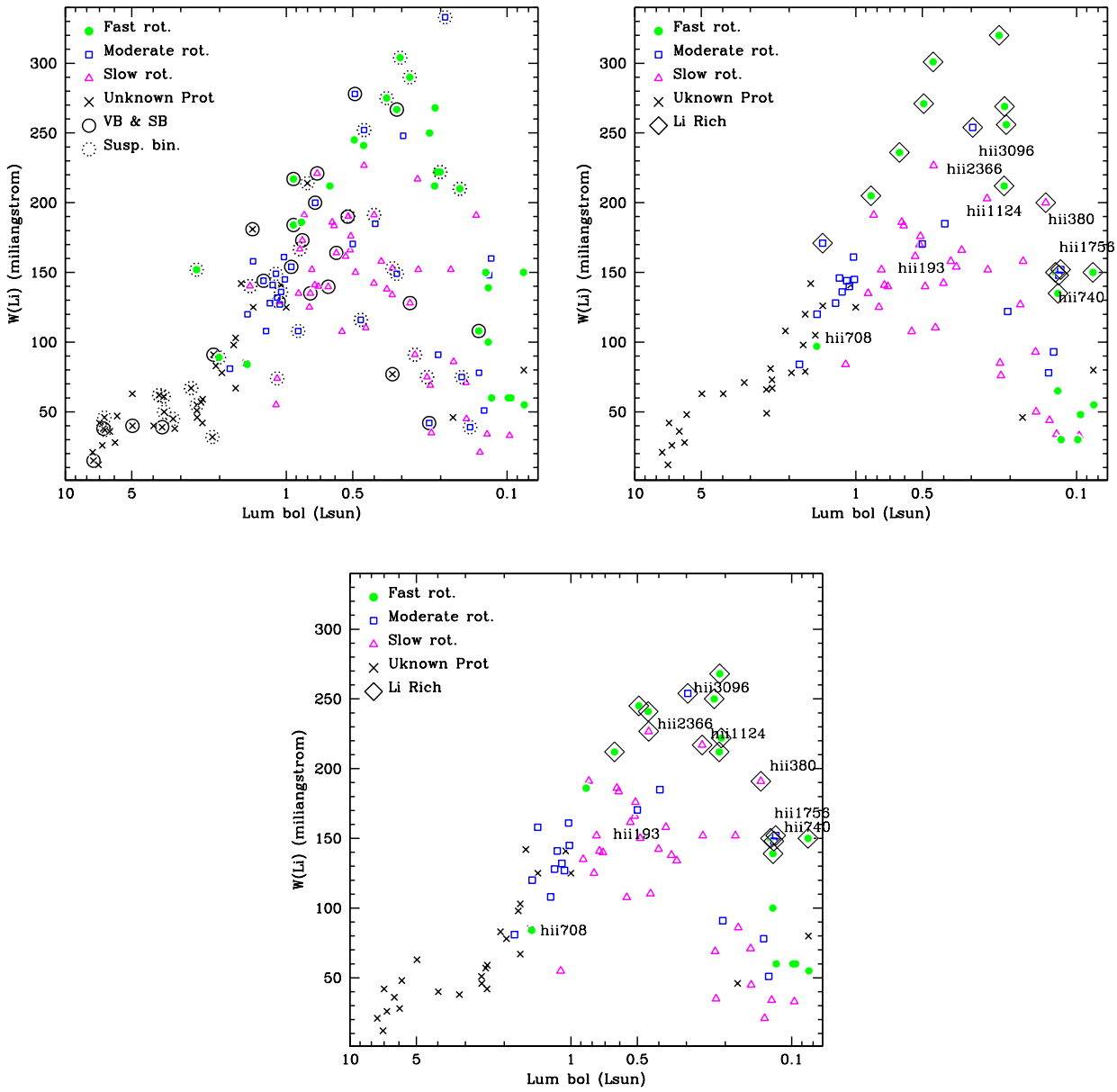

Fig. 6. Lithium equivalent with versus the bolometric luminosity for the high probable members (probability larger than 0.75). For those stars with multiple values of W(Li), only our selection is represented (see text). **Top:** Binaries and suspected binaries are included and highlighted with large open circles. **Middle and bottom:** Only single stars are displayed. Lithium-rich stars are also indicates with large, open diamonds. In the first case we have used the W(Li) selection based on the S/N –selection B– whereas in the second panel we display the data based on spectral resolution –selection A.

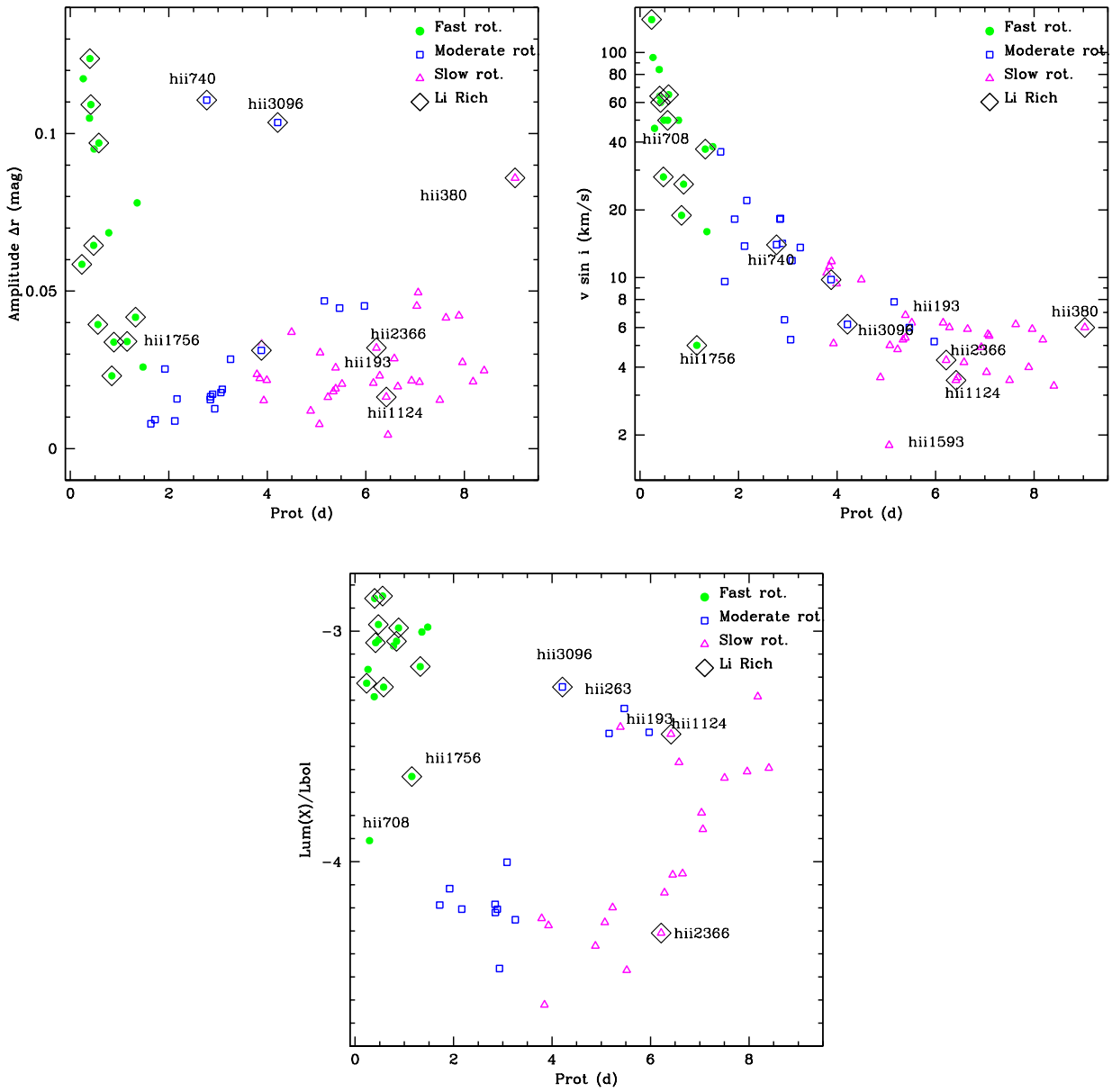

Fig. 7. Photometric variability in the *r* band (**top**). the projected equatorial velocity (**middle**), and the fraction between the Lx and the bolometric luminosities (**bottom**) versus the rotational period. Only single stars are displayed. The lithium rich stars come from selection A, based on spectral resolution, although the result is practically identical if the stress is put on the S/N. Note that HII380 and HII740 do not have a measured value of Lx, and HII708 does not have a measured value of the photometric amplitude, and therefore they are not represented on some of these diagrams.

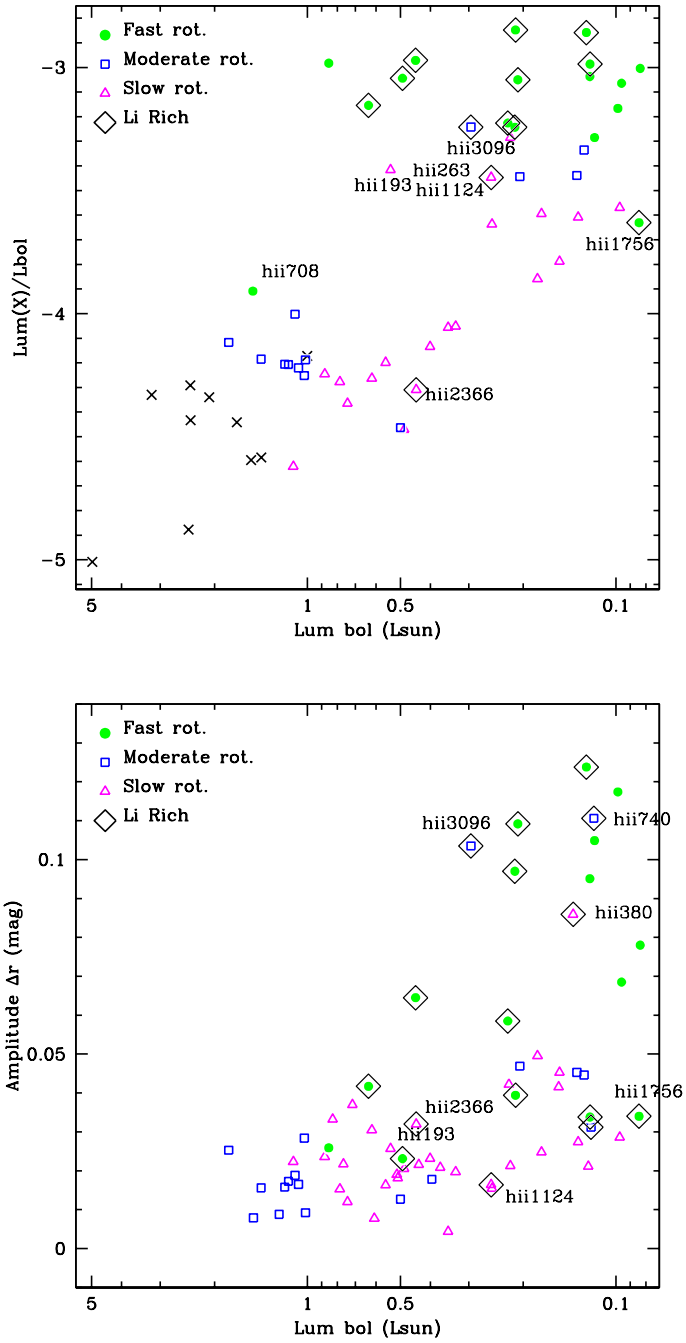

Fig. 8. Top.- Comparison of the X-ray and the bolometric luminosities, taking into account the rotational periods. Note that HII380 and HII740 do not have a measured value of Lx and therefore they are not represented on the diagram. **Bottom.-** The amplitude of the light curve. Only single stars and the W(Li) based on the spectral resolution are displayed in both panels.

Table 1. Complete compilation of the Lithium equivalent width.

Name	RA (deg)	DEC (deg)	WLi-F[1] (mÅ)	eWLi-F (mÅ)	Source	WLi[2] Ki10	WLi[3] Jo96	eWLi	WLi[4] Op97	WLi[5] So93	WLi[6] Ma07	WLi[7] Je99	eWLi	WLi[8] GL94	eWLi	SNR Ki10	SNR Ma07
BPL163	56.993000	22.114194	≤70	–	Da15	–	–	–	–	–	–	–	–	–	–	–	–
BPL327	58.846125	24.818139	≤200	–	Da15	–	–	–	–	–	–	–	–	–	–	–	–
LZJ-50	55.983292	25.607083	≤70	–	Da15	–	–	–	–	–	–	–	–	–	–	–	–
PPL-14	56.142833	23.856917	350	90	Da15	–	–	–	–	–	–	–	–	–	–	–	–
AK I-1-317	58.589973	24.075645	78	10	Ma07	–	–	–	–	–	78	–	–	–	–	–	230
AK II-437	54.921543	23.290886	142	10	Ma07	–	–	–	–	–	142	–	–	–	–	–	145
AK III-756	55.400673	25.619331	120	10	Ma07	–	–	–	–	–	120	–	–	–	–	–	155
AK V-595	60.934029	22.944309	32	10	Ma07	–	–	–	–	–	32	–	–	–	–	–	200
CFHT-PL-09[a]	57.312916	24.606222	≤50.0	–	St98	–	–	–	–	–	–	–	–	–	–	–	–
CFHT-PL-10	56.134583	25.421722	≤50.0	–	St98	–	–	–	–	–	–	–	–	–	–	–	–
CFHT-PL-11	56.9125	24.606138	500	–	St98	–	–	–	–	–	–	–	–	–	–	–	–
CFHT-PL-12	58.479584	23.393723	800	–	St98	–	–	–	–	–	–	–	–	–	–	–	–
CFHT-PL-14	55.809166	24.38925	<100	–	St98	–	–	–	–	–	–	–	–	–	–	–	–
CFHT-PL-15	58.802082	23.293888	500	–	St98	–	–	–	–	–	–	–	–	–	–	–	–
CFHT-PL-16	56.146667	25.228695	1200	0.0	Mt00	–	–	–	–	–	–	–	–	–	–	–	–
CFHT-PL-18	58.34625	23.322083	≤200	–	Mt00	–	–	–	–	–	–	–	–	–	–	–	–
Calar-03	57.856667	23.755722	1800	400	Re96	–	–	–	–	–	–	–	–	–	–	–	–
Lick-PL-01	57.05958	24.264168	≤100	–	St98	–	–	–	–	–	–	–	–	–	–	–	–
MHObd3	55.475456	23.084862	800	–	St98	–	–	–	–	–	–	–	–	–	–	–	–
PPl-01	56.422085	23.903334	1800	–	St98	–	–	–	–	–	–	–	–	–	–	–	–
PPl-15	57.020084	23.65889	500	100	Ba96	–	–	–	–	–		–	–	–	–	–	–
Pels041	56.183105	25.499289	199	10	So93	–	–	–	–	199	–	–	–	–	–	–	–
Pels043	55.954216	25.729616	225	10	So93	–	–	–	–	225	–	–	–	–	–	–	–
Pels112	58.618523	24.321157	70	10	So93	–	–	–	–	70	–	–	–	–	–	–	–
Pels124	53.88203	22.823627	98	10	Ma07	–	–	–	–	–	98	–	–	–	–	–	195
Pels173	60.221325	23.193913	57	10	Ma07	–	–	–	–	–	57	–	–	–	–	–	220
Pels192	58.870853	23.772451	80	10	So93	–	–	–	–	80	–	–	–	–	–	–	–
Roque05	56.09354	23.65036	≤8000	–	Mt98	–	–	–	–	–	–	–	–	–	–	–	–
Roque12	57.07921	24.420279	≤1500	–	Mt98	–	–	–	–	–	–	–	–	–	–	–	–
Roque13	56.460835	24.150833	2500	–	St98	–	–	–	–	–	–	–	–	–	–	–	–
Roque25	57.128082	22.747278	≤5000	–	Mt98	–	–	–	–	–	–	–	–	–	–	–	–
Roque33	57.204666	24.34039		–	Pi03	–	–	–	–	–	–	–	–	–	–	–	–
Teide01	56.82458	24.375528	1000	200	Re96	–	–	–	–	–	–	–	–	–	–	–	–
Teide02[b]	58.027916	24.266945	770	150	Ma98	–	–	–	–	–	–	–	–	–	–	–	–
HCG0131[c]	56.011784	25.656338	407	10	Ma07	–	–	–	–	–	407	–	–	–	–	–	120
HCG0332	57.110798	23.191612	900	–	Op97	–	–	–	900	–	–	–	–	–	–	–	–
HCG0509	59.126217	24.288831	700	–	Op97	–	–	–	700	–	–	–	–	–	–	–	–
HHJ0003	57.210144	22.741737	≤190	–	Ma94	–	–	–	≤190	–	–	–	–	–	–	–	–
HHJ0006	55.426693	23.915899	≤50.0	–	Op97	–	–	–	≤50	–	–	–	–	–	–	–	–
HHJ0010	57.146606	22.895149	≤50.0	–	Op97	–	–	–	≤50	–	–	–	–	–	–	–	–
HHJ0011	56.503819	22.208258	≤50.0	–	Op97	–	–	–	≤50	–	–	–	–	–	–	–	–
HHJ0014	56.302544	23.895882	≤180	–	Ma94	–	–	–	≤180	–	–	–	–	–	–	–	–
HHJ0016	56.874683	23.554222	≤50.0	–	Op97	–	–	–	≤50	–	–	–	–	–	–	–	–
HHJ0018	55.777054	22.297075	≤50.0	–	Op97	–	–	–	≤50	–	–	–	–	–	–	–	–
HHJ0019	54.315	26.492028	≤50.0	–	Op97	–	–	–	≤50	–	–	–	–	–	–	–	–
HHJ0036	57.315067	23.380386	≤50.0	–	Op97	–	–	–	≤50	–	–	–	–	–	–	–	–
HII0025	55.729626	24.493065	57	10	So93	–	–	–	–	57	81	–	–	–	–	–	580
HII0034	55.76223	24.669737	134	10	So93	–	–	–	–	134	166	147, 154	5, 7	–	–	–	250
HII0097	55.860924	24.994333	75.0	5.0	Jo96	–	75	5	–	79	78, 69	–	–	38	0	–	150, 190
HII0102	55.852238	23.225933	149	10	So93	–	–	–	–	149	–	–	–	–	–	–	–
HII0120	55.883141	23.674074	152	10	So93	–	–	–	–	152	–	–	–	–	–	–	–
HII0129	55.893372	23.761917	176	10	So93	–	–	–	–	176	–	–	–	–	–	–	–
HII0133	55.903843	24.393944	55.0	5.0	Jo96	–	55	5	–	–	–	–	–	–	–	–	–

Table 1. continued.

NameF	RAdegF (deg)	DECdegF (deg)	WLi-F (mÅ)	eWLi-F (mÅ)	Source	WLi[2] K10	WLi[3] Jo96	eWLi Jo96	WLi[4] Op97	WLi[5] So93	WLi[6] Ma07	WLi[7] Je99	eWLi Je99	WLi[8] GL94	eWLi GL94	SNR Ki10	SNR Ma07
HII0152	55.907204	23.536011	191.2	10	Ki10	191.2	–	–	–	150	–	–	–	–	–	96	–
HII0158	55.93021	24.37455	36	10	Ma07	–	–	–	–	–	36	–	–	–	–	–	440
HII0164	55.928608	23.594801	59	10	So93	–	–	–	–	59	67	–	–	–	–	–	130
HII0173	55.951721	25.190042	260	10	So93	–	–	–	–	260	173	–	–	–	–	–	260
HII0174	55.951378	25.004387	241	10	So93	–	–	–	–	241	270, 332	290, 299	11, 12	–	–	–	500, 165
HII0193	55.961273	24.247465	161.5	10	Ki10	161.5	–	–	–	148	160	–	–	–	–	100	330
HII0232	56.001106	24.55695	15	10	Ma07	–	–	–	–	–	15	–	–	–	–	–	620
HII0233	55.995003	23.88273	75	10	So93	–	–	–	–	75	91	–	–	–	–	–	230
HII0248	56.002472	23.543961	193	10	So93	–	–	–	–	193	–	–	–	–	–	–	–
HII0250	56.017681	24.989822	166.7	10	Ki10	166.7	–	–	–	141	162, 156	–	–	–	–	97	680, 290
HII0253	56.014748	24.504206	186	10	So93	–	–	–	–	186	205	–	–	–	–	–	575
HII0263	56.020168	24.275501	252.1	10	Ki10	252.1	–	–	–	290	264	240	5	–	–	133	400
HII0293	56.05798	24.779388	125	10	So93	–	–	–	–	125	–	–	–	–	–	–	–
HII0296	56.046692	23.37933	278	10	So93	–	–	–	–	278	–	–	–	–	–	–	–
HII0298	56.05253	24.031786	266.8	10	Ki10	266.8	–	–	–	277	–	–	–	–	–	80	–
HII0303	56.061119	24.101816	138	10	So93	–	–	–	–	138	153	–	–	–	–	–	305
HII0314	56.083687	24.796156	167	10	So93	–	–	–	–	167	184	–	–	–	–	–	554
HII0320	56.085445	24.772854	221	10	So93	–	–	–	–	221	–	–	–	233	15	–	–
HII0324	56.09127	24.768408	210	20	Jo96	–	210	20	–	–	202	–	–	288	20	–	265
HII0335	56.096096	24.068304	≤20	–	GL94	–	–	–	–	–	–	–	–	≤220	–	–	–
HII0338	56.09811	24.132639	50	10	So93	–	–	–	–	50	76	–	–	–	–	–	475
HII0344	56.107113	24.394674	26	10	Ma07	–	–	–	–	–	26	–	–	–	–	–	620
HII0345	56.109486	24.589705	245	10	So93	–	–	–	–	245	271	270, 282	5, 10	–	–	–	340
HII0347	56.113724	24.843962	≤40	–	Jo96	–	≤40	–	–	–	–	–	–	≤215	–	–	–
HII0380	56.155899	25.137793	191	10	So93	–	–	–	–	191	191, 198, 202, 209	–	–	212	5	–	100, 130, 200, 205
HII0405	56.1698	24.818542	81	10	So93	–	–	–	–	81	84	–	–	–	–	–	330
HII0430	56.18325	24.231215	150	10	So93	–	–	–	–	150	140	–	–	–	–	–	360
HII0470	56.213482	23.268969	62	10	So93	–	–	–	–	62	83	–	–	–	–	–	160
HII0476	56.224304	23.921267	108	10	So93	–	–	–	–	108	–	–	–	–	–	–	–
HII0489	56.234989	24.432623	127	10	So93	–	–	–	–	127	136, 143	–	–	–	–	–	410, 400
HII0514	56.266689	25.257841	135	10	So93	–	–	–	–	135	–	–	–	–	–	–	–
HII0522	56.263603	23.839439	77	10	So93	–	–	–	–	77	–	–	–	–	–	–	–
HII0530	56.272011	23.702707	61	10	So93	–	–	–	–	61	76	–	–	–	–	–	165
HII0531	56.277229	24.263523	63	10	Ma07	–	–	–	–	–	73, 52	–	–	–	–	–	500, 620
HII0571	56.313946	25.289476	164.0	10	Ki10	164.0	–	–	–	175	169, 175	–	–	–	–	126	250, 255
HII0605	56.336918	24.922075	39	10	So93	–	–	–	–	39	61, 64	–	–	–	–	–	560, 655
HII0625	56.338284	23.727499	290	25.	GL94	–	–	–	–	–	–	–	–	290	25	–	–
HII0627	56.350533	24.885977	83	10	So93	–	–	–	–	83	111, 104	–	–	–	–	–	440, 370
HII0636	56.34248	23.471731	152	10	So93	–	–	–	–	152	–	–	–	–	–	–	–
HII0652	56.358902	24.035139	21	10	Ma07	–	–	–	–	–	21, 0	–	–	–	–	–	500, 660
HII0676	56.373203	23.760529	34	5	Jo96	–	34	5	–	–	–	–	–	–	–	–	–
HII0686	56.387222	24.303242	150	20	Jo96	–	150	20	–	–	–	–	–	130	10	–	–
HII0697	56.393559	24.463299	30	10	So93	–	–	–	–	30	47, 52	–	–	–	–	–	635, 460
HII0708	56.397484	24.08321	84	10	So93	–	–	–	–	84	98, 95	–	–	–	–	–	420, 395
HII0727	56.41737	24.627245	89	10	So93	–	–	–	–	89	94, 105, 104	–	–	–	–	–	550, 435, 210
HII0738	56.4142	23.754284	203	10	So93	–	–	–	–	203	–	–	–	–	–	–	–
HII0739	56.42548	24.905998	152	10	So93	–	–	–	–	152	160, 158	–	–	–	–	–	480, 555
HII0740	56.426872	25.057091	152	10	Ma07	–	–	–	–	–	160, 144	–	–	–	–	–	155, 155
HII0745	56.422436	24.288599	55	10	Ma07	–	–	–	–	–	55, 54	–	–	–	–	–	625, 300
HII0746	56.424374	24.431513	107.6	10	Ki10	107.6	–	–	–	98	–	–	–	–	–	140	–
HII0761	56.43504	24.220335	154	10	So93	–	–	–	–	154	–	–	–	–	–	–	–
HII0870	56.511482	23.737392	149	10	So93	–	–	–	–	149	–	–	–	–	–	–	–
HII0879	56.527061	24.567419	152	10	So93	–	–	–	–	152	124, 130	–	–	116	0	–	115, 135
HII0882	56.517178	23.405537	212	10	So93	–	–	–	–	212	–	–	–	–	–	–	–

Table 1. continued.

NameF	RAdegF (deg)	DECdegF (deg)	WLi-F (mÅ)	eWLi-F (mÅ)	Source	WLi[2] K10	WLi[3] Jo96	eWLi Jo96	WLi[4] Op97	WLi[5] So93	WLi[6] Ma07	WLi[7] Je99	eWLi Je99	WLi[8] GL94	eWLi GL94	SNR Ki10	SNR Ma07
HII0883	56.528744	24.562807	45	10	So93	–	–	–	–	45	50	–	–	–	–	–	150
HII0885	56.53236	24.866802	148	10	So93	–	–	–	–	148	154	–	–	–	–	–	250
HII0916	56.548939	24.622314	191.3	10	Ki10	191.3	–	–	–	199	206, 189	185, 187	4, 9	–	–	109	205, 355
HII0923	56.541874	23.340015	158	10	So93	–	–	–	–	158	171	–	–	–	–	–	295
HII0974	56.585312	24.78548	33	8.0	GL94	–	–	–	–	–	–	–	–	33	8	–	–
HII0975	56.574959	23.486664	74	10	So93	–	–	–	–	74	–	–	–	–	–	–	–
HII0996	56.594479	24.570177	132	10	So93	–	–	–	–	132	142, 146	–	–	–	–	–	310, 315
HII1005	56.60015	24.361542	46	10	Ma07	–	–	–	–	–	46	–	–	–	–	–	100
HII1015	56.613968	25.135563	145	10	So93	–	–	–	–	145	–	–	–	–	–	–	–
HII1032	56.618378	24.433918	212	10	So93	–	–	–	–	212	236	–	–	–	–	–	500
HII1039	56.615738	23.592699	333	10	So93	–	–	–	–	333	320, 322	–	–	–	–	–	110, 165
HII1084	56.642521	23.62401	0.0	10	Ma07	–	–	–	–	–	0	–	–	–	–	–	655
HII1095	56.657391	24.747698	138	10	So93	–	–	–	–	138	157, 150	130	6	–	–	–	200, 275
HII1100	56.655285	24.343527	153	10	So93	–	–	–	–	153	158	–	–	–	–	–	100
HII1101	56.661587	24.959629	144	10	So93	–	–	–	–	144	–	–	–	–	–	–	–
HII1103	56.647205	23.411737	≤20	–	GL94	–	–	–	–	–	–	–	–	≤20	–	–	–
HII1110	56.662018	24.520338	21	10	So93	–	–	–	–	21	44	–	–	–	–	–	87
HII1117	56.656994	23.787771	159	10	So93	–	–	–	–	159	181	–	–	–	–	–	290
HII1122	56.663857	24.103243	67	10	So93	–	–	–	–	67	85	–	–	–	–	–	525
HII1124	56.664104	24.029688	217	10	So93	–	–	–	–	217	203	189	7	220	5	–	140
HII1132	56.659985	22.919804	46	10	So93	–	–	–	–	46	49	–	–	–	–	–	575
HII1136	56.667671	23.497789	275	20	Jo96	–	275	20	–	295	–	–	–	–	–	–	–
HII1139	56.666656	23.110371	51	10	So93	–	–	–	–	51	66	–	–	–	–	–	500
HII1182	56.696087	22.914593	136	10	So93	–	–	–	–	136	156	–	–	–	–	–	290
HII1200	56.710571	23.239195	67	10	So93	–	–	–	–	67	79	–	–	–	–	–	395
HII1207	56.728828	24.796349	141	10	So93	–	–	–	–	141	–	–	–	–	–	–	–
HII1215	56.723911	23.583599	125	10	So93	–	–	–	–	125	–	–	–	–	–	–	–
HII1220	56.72192	22.880943	158	10	So93	–	–	–	–	158	–	–	–	–	–	–	–
HII1266	56.764782	24.819933	39	10	Ma07	–	–	–	–	–	46, 32	–	–	–	–	–	500, 500
HII1275	56.755909	23.494984	159	10	So93	–	–	–	–	159	174	–	–	–	–	–	305
HII1284	56.767551	23.995174	48	10	Ma07	–	–	–	–	–	49, 47	–	–	–	–	–	565, 575
HII1298	56.778252	23.71517	91	10	So93	–	–	–	–	91	98	–	–	–	–	–	315
HII1305	56.780609	23.226339	≤60	–	Jo96	–	≤60	–	–	30	0	–	–	≤250	–	–	180
HII1306	56.78558	23.710819	75	5	Jo96	–	75	5	–	64	–	–	–	–	–	–	–
HII1309	56.791893	24.276672	42	10	So93	–	–	–	–	42	73	–	–	–	–	–	590
HII1332	56.806374	23.71431	35	10	So93	–	–	–	–	35	76	–	–	73	6	–	155
HII1338	56.819008	24.128347	40	10	Ma07	–	–	–	–	–	43, 36	–	–	–	–	–	460, 460
HII1348	56.825268	24.390772	42	10	Ma07	–	–	–	–	–	42	–	–	–	–	–	120
HII1362	56.830624	24.139126	28	10	Ma07	–	–	–	–	–	28	–	–	–	–	–	620
HII1407	56.845417	22.922121	12	10	Ma07	–	–	–	–	–	12	–	–	–	–	–	800
HII1454	56.89032	24.684223	86	10	So93	–	–	–	–	86	158	–	–	104	0	–	110
HII1514	56.918537	24.364594	161	10	So93	–	–	–	–	161	–	–	–	–	–	–	–
HII1531	56.922657	23.971945	100	10	So93	–	–	–	–	100	61, 67,66	–	–	≤260	–	–	115, 160, 140
HII1532	56.921581	23.740294	60	20	Jo96	–	60	20	–	–	33, 62	–	–	52	10	–	125, 170
HII1553	56.920734	22.930014	304	10	So93	–	–	–	–	304	–	–	–	–	–	–	–
HII1593	56.950462	23.21814	183.5	10	Ki10	183.5	–	–	–	164	176	–	–	–	–	128	260
HII1613	56.968838	23.941282	103	10	So93	–	–	–	–	103	122, 118	–	–	–	–	–	420, 3530
HII1653	56.998894	24.731342	108	10	So93	–	–	–	–	108	55, 52	–	–	–	–	–	130, 150
HII1726	57.029949	24.142099	94	10	So93	–	–	–	–	94	112, 11	–	–	–	–	–	350, 555
HII1756	57.045776	23.507023	150	20	Jo96	–	150	20	–	–	–	–	–	–	–	–	–
HII1762	57.05645	24.318428	37	10	Ma07	–	–	–	–	–	37	–	–	–	–	–	620
HII1766	57.070267	25.21517	45	10	So93	–	–	–	–	45	58	–	–	–	–	–	570
HII1776	57.073719	25.047886	140	10	So93	–	–	–	–	140	–	–	–	–	–	–	–
HII1794	57.071342	23.890385	55	10	So93	–	–	–	–	55	84	–	–	–	–	–	415

Table 1. continued.

NameF	RAdegF (deg)	DECdegF (deg)	WLi-F (mÅ)	eWLi-F (mÅ)	Source	WLi[2] K10	WLi[3] Jo96	eWLi Jo96	WLi[4] Op97	WLi[5] So93	WLi[6] Ma07	WLi[7] Je99	eWLi Je99	WLi[8] GL94	eWLi GL94	SNR Ki10	SNR Ma07
HII1797	57.070457	23.636806	125	10	So93	–	–	–	–	125	126	–	–	–	–	–	350
HII1856	57.109024	24.048445	85	10	So93	–	–	–	–	85	113, 99, 102	–	–	–	–	–	255, 320, 430
HII1883	57.116787	23.300774	250	20	Jo96	–	250	20	–	282	320	–	–	251	0	–	245
HII1912	57.145004	24.181202	71	10	So93	–	–	–	–	71	82, 79, 112	–	–	–	–	–	490, 470, 600
HII1924	57.143806	23.434818	141	10	So93	–	–	–	–	141	139, 133	–	–	–	–	–	285, 700
HII2016	57.189312	23.338873	148	10	So93	–	–	–	–	148	–	–	–	–	–	–	–
HII2027	57.203949	24.267435	135	10	So93	–	–	–	–	135	–	–	–	–	–	–	–
HII2034	57.205509	23.97732	222	10	So93	–	–	–	–	222	226, 248	220, 230	13, 19	238	0	–	290, 280
HII2106	57.24369	23.201229	116	10	So93	–	–	–	–	116	125, 134	–	–	–	–	–	275, 215
HII2126	57.259705	23.252468	184.9	10	Ki10	184.9	–	–	–	151	186, 183	–	–	–	–	119	245, 175
HII2147	57.275452	23.781273	217	10	So93	–	–	–	–	217	–	–	–	–	–	–	–
HII2172	57.298859	24.636606	129	10	So93	–	–	–	–	129	–	–	–	–	–	–	–
HII2193	57.296989	23.555243	≤60	–	Jo96	–	≤60	–	–	–	–	–	–	–	–	–	–
HII2195	57.300808	23.886839	38	10	Ma07	–	–	–	–	–	48, 28	–	–	–	–	–	680, 420
HII2208	57.314083	24.567284	≤60	–	Jo96	–	≤60	–	–	–	–	–	–	–	–	–	–
HII2244	57.335793	24.77667	268	10	So93	–	–	–	–	268	269	–	–	251	0	–	130
HII2278	57.357094	24.93762	214	10	So93	–	–	–	–	214	–	–	–	–	–	–	–
HII2281	57.34875	23.880833	184	10	So93	–	–	–	–	184	–	–	–	–	–	–	–
HII2284	57.350216	23.839287	190.3	10	Ki10	190.3	–	–	–	177	192, 198	–	–	–	–	105	275, 185
HII2311	57.369747	23.712238	170.4	10	Ki10	170.4	–	–	–	141	154	–	–	–	–	114	300
HII2341	57.388004	23.795427	141	10	So93	–	–	–	–	141	–	–	–	–	–	–	–
HII2345	57.386341	23.380413	38	10	So93	–	–	–	–	38	71	–	–	–	–	–	465
HII2366	57.402245	24.296135	226.7	10	Ki10	226.7	–	–	–	189	218	–	–	–	–	81	245
HII2406	57.414158	23.290129	139.7	10	Ki10	139.7	–	–	–	154	147, 150	–	–	–	–	150	310, 265
HII2407	57.426128	24.46306	125	10	So93	–	–	–	–	125	128	116, 125	7, 5	–	–	–	220
HII2415	57.420506	23.341612	42	10	Ma07	–	–	–	–	–	42, 41	–	–	–	–	–	520, 740
HII2462	57.459827	23.705631	110.3	10	Ki10	110.3	–	–	–	103	108, 113	–	–	–	–	110	400, 315
HII2506	57.485363	23.218641	108	10	So93	–	–	–	–	108	128	–	–	–	–	–	225
HII2588	57.551674	24.532957	78	10	So93	–	–	–	–	78	71, 84, 80, 77	–	–	–	–	–	140, 100, 210, 120
HII2644	57.587078	24.466755	186	10	So93	–	–	–	–	186	–	–	–	–	–	–	–
HII2665	57.588753	23.096392	166	10	So93	–	–	–	–	166	170	–	–	–	–	–	300
HII2741	57.644051	24.507822	91	10	So93	–	–	–	–	91	120, 124	–	–	107	0	–	195, 105
HII2786	57.666985	23.933065	128	10	So93	–	–	–	–	128	146	–	–	–	–	–	303
HII2870	57.714333	23.3291	69	10	So93	–	–	–	–	69	85	–	–	–	–	–	225
HII2880	57.729527	24.197466	142.3	10	Ki10	142.3	–	–	–	122	133	–	–	–	–	84	340
HII2881	57.726337	23.834896	190	10	Ma07	–	–	–	–	–	190	–	–	–	–	–	185
HII2908	57.759632	25.055477	193	10	Ma07	–	–	–	–	–	196, 191	–	–	–	–	–	95, 160
HII2927	57.773258	24.736776	≤60	–	Jo96	–	≤60	–	–	–	0	–	–	30	0	–	200
HII2984	57.820232	23.826605	64	10	Ma07	–	–	–	–	–	64	–	–	–	–	–	245
HII3019	57.851673	24.087425	51	10	So93	–	–	–	–	51	87, 99	–	–	71	0	–	150, 120
HII3031	57.863419	24.518692	40	10	So93	–	–	–	–	40	63	–	–	–	–	–	450
HII3063	57.874737	23.899223	139	10	So93	–	–	–	–	139	142, 127	–	–	–	–	–	105, 165
HII3096	57.913651	24.548941	254	10	Ma07	–	–	–	–	–	260, 248	–	–	–	–	–	145, 260
HII3097	57.918503	24.983185	198	10	So93	–	–	–	–	198	200	–	–	–	–	–	230
HII3104	57.908424	23.18317	39	10	Ma07	–	–	–	–	–	39	–	–	–	–	–	140
HII3163	57.972446	24.387018	222	10	So93	–	–	–	–	222	256	–	–	238	0	–	175
HII3179	57.986889	23.901966	140.2	10	Ki10	140.2	–	–	–	121	158	–	–	–	–	158	295
HII3187	57.988895	23.339439	71	10	So93	–	–	–	–	71	93	–	–	–	–	–	205
HII3197	58.009331	24.663309	302	10	So93	–	–	–	–	302	270	–	–	–	–	–	100

Lithium references by priority: Ki10 = King et al. (2010), Jo96 = Jones et al. (1996), Op97 = Oppenheimer et al. (1997), So93 = Soderblom et al. (1993b), Ma07 = Margheim (2007), Je99 = Jeffries (1999), GL94 = Garcia Lopez et al. (1994),

[1] Selected lithium equivalent width.

[2] The errors can be estimated as 10 mÅ in King et al. (2010).

[3] The FeI6707.4 Å line does not contributed to the listed W(Li). The errors can be estimated as 5 and 20 mÅ for slow and fast rotators (Jones et al. 1996).
[4] If present, the LiI6708 Å feature dominates the region for these mid-M dwarfs in Oppenheimer et al. (1997).
[5] The FeI6707.4 Å line does not contributed to the listed W(Li). The errors can be estimated as 10 mÅ in Soderblom et al. (1993b), based on their comparison with previous data.
[6] R~12500. W(Li) includes the contribution by FeI6707.4 Å. The errors have been estimated as 10 m for the ÅMargheim (2007) data. The quoted internal errors are 1-2 mÅ
[7] SNR=80-110, R~14500. W(Li) after removing the FeI contribution, as listed in Jeffries (1999).
[8] R~10000. We include the W(Li) as listed in Garcia Lopez et al. (1994), since the FeI6707.4 Å contribution was eliminated in that paper.
[a] CFHT-PL-09: W(Li)≤60 mÅ in Dahm (2015).
[b] Teide02 = CFHT-PL-13: (Li)=600 mÅ in Stauffer et al. (1998a) and W(Li)=520±130 mÅ in Dahm (2015).
[c] HCG0131 is listed as HCG 938 in Margheim (2007), which does not exist. After checking the available data we believe the fiber was allocated to HCG 131.

Table 2. Proper motions and membership probabilities for the Pleiades lithium sample. Only single stars with membership probability larger than 0.75, after removing binaries and suspected binaries.

Name	RA (deg)	DEC (deg)	pmRA (arcsec)	pmDEC (arcsec)	epmRA (arcsec)	epmDE (arcsec)	Prob[1] All	Prob[2] PM	Source[3] PM	Other names
BPL163	56.991825	22.114128	17.74	-39.84	0.19	0.19	1.0	0.9	D, ?: D	
BPL327	58.846134	24.818094	20.17	-40.73	0.38	0.38	1.0	0.6	D, ?: D	HHJ I-14, PLZJ78
LZJ-50	55.98334	25.607027	16.97	-41.44	0.32	0.32	1.0	0.93	D, ?: D	
PPL-14	56.142925	23.856792	17.0	-38.82	0.45	0.45	1.0	0.9	D, ?: D	
AK I-1-317	58.589973	24.075645	19.7	-46.0	0.9	1.0	1.0	0.97	D, T: T	AK1A317 HD24463
AK II-437	54.921543	23.290886	22.2	-43.7	1.0	1.1	1.0	0.92	D, T: T	PELS017 HD22680 AK 2437
AK III-756	55.400673	25.619331	21.1	-44.7	1.7	1.7	1.0	0.95	D, T: T	PELS023 DH181 AK 3756
CFHT-PL-11	56.9125	24.606138	17.29	-41.97	0.14	0.14	1.0	0.92	D, ?: D	Roque16 BRB12 BPL152
CFHT-PL-12	58.479584	23.393723	14.72	-38.74	0.14	0.14	1.0	0.89	D, ?: D	BPL294 PLIZ6 BRB9 PLZJ9
CFHT-PL-16	56.146667	25.228695	15.63	-42.0	0.18	0.18	1.0	0.9	D, ?: D	PLIZ9
Calar-03	57.856667	23.755722	15.47	-40.72	0.23	0.23	1.0	0.92	D, ?: D	CFHT-PL-21 BRB14 PLIZ12 BPL235
PPl-15	57.020084	23.65889	11.75	-36.47	0.65	0.65	1.0	0.36	D, ?: D	NPL35 SHF48 IPMBD23
Pels124	53.88203	22.823627	21.0	-44.4	1.2	1.3	1.0	0.96	D, T: T	PELS124
Pels192	58.870853	23.772451	14.61	-40.75	0.53	0.53	0.99	0.88	D, ?: D	PELS192 HCG498
Roque13	56.460835	24.150833	15.2	-38.17	0.46	0.46	1.0	0.89	D, ?: D	BPL79 SHF19
Teide01	56.82458	24.375528	14.39	-38.91	0.65	0.65	1.0	0.87	D, ?: D	BPL137 NPL39
Teide02	58.027916	24.266945	18.62	-42.4	0.14	0.14	1.0	0.85	D, ?: D	CFHT-PL-13 BPL254 PLIZ3 PLZJ46 BRB11
HCG0332	57.110798	23.191612	23.99	-36.63	0.14	0.14	0.89	0.07	D, ?: D	HCG332 SK362 HHJ339
HII0025	55.729626	24.493065	19.9	-43.2	1.1	1.1	1.0	0.96	D, T: T	HII25 HD23061 TrR11
HII0034	55.76223	24.669737	21.8	-48.8	3.7	3.7	0.93	0.88	D, T: T	HII34 DH250
HII0097	55.860924	24.994333	20.97	-39.43	0.25	0.25	1.0	0.33	D, ?: D	HII97 HCG108 DH266
HII0120	55.88314	23.674074	20.7	-46.7	1.5	1.5	1.0	0.95	D, T: T	HII120 Tr37
HII0129	55.89337	23.761917	20.2	-45.1	2.4	2.5	0.99	0.94	D, T: T	HII129 Tr041 DH271
HII0133	55.903843	24.393944	15.81	-38.9	0.15	0.15	0.98	0.92	D, ?: D	HII133 HCG118 SK625 DH277
HII0152	55.907204	23.53601	19.4	-47.8	2.0	2.1	0.99	0.94	D, T: T	HII152 Tr46
HII0158	55.93021	24.37455	18.0	-43.9	1.0	0.9	1.0	0.94	?, T: T	HII158 HD23156 Tr51
HII0164	55.928608	23.5948	21.4	-45.6	1.1	1.0	0.99	0.96	D, T: T	HII164 HD23158 Tr53
HII0174	55.951378	25.004387	22.0	-45.7	2.0	2.1	1.0	0.93	D, T: T	HII174 Tr56
HII0193	55.961273	24.247465	22.0	-47.4	1.8	1.9	0.99	0.92	D, T: T	HII193 Tr060
HII0250	56.01768	24.989822	16.6	-47.1	1.8	1.8	0.99	0.88	D, T: T	HII250 Tr080
HII0253	56.014748	24.504206	24.4	-45.0	1.9	2.1	0.99	0.81	D, T: T	HII253 Tr081 DH309
HII0263	56.02017	24.275501	14.59	-47.06	0.42	0.42	1.0	0.31	D, ?: D	HII263 Tr089
HII0293	56.05798	24.779388	21.2	-46.0	1.8	1.8	1.0	0.95	D, T: T	HII293 Tr098
HII0324	56.09127	24.768408	15.72	-43.32	0.68	0.68	1.0	0.83	D, ?: D	HII324 HCG147 DH328
HII0344	56.107113	24.394674	22.7	-48.7	1.1	1.0	0.99	0.85	D, T: T	HII344 HD23246 Tr121
HII0345	56.109486	24.589705	8.79	-56.42	0.69	0.69	1.0	0.0	D, ?: D	HII345 Tr122
HII0380	56.1559	25.137793	21.0	-38.87	2.53	2.53	1.0	0.6	D, ?: D	HII380 DH349
HII0405	56.1698	24.818542	17.0	-46.3	1.5	1.5	1.0	0.91	?, T: T	HII405 HD23269 Tr131
HII0430	56.18325	24.231215	22.12	-43.55	0.75	0.75	1.0	0.24	D, ?: D	HII430 Tr137
HII0470	56.21348	23.268969	20.4	-42.2	0.9	0.9	0.99	0.92	D, T: T	HII470 HD23289 Tr149
HII0489	56.23499	24.432623	14.36	-44.23	0.63	0.63	1.0	0.57	D, ?: D	HII489 Tr153
HII0514	56.26669	25.257841	18.0	-43.5	1.6	1.6	0.98	0.93	D, T: T	HII514 DH370

Table 2. continued.

Name	RA (deg)	DEC (deg)	pmRA (arcsec)	pmDEC (arcsec)	epmRA (arcsec)	epmDE (arcsec)	Prob[1] All	Prob[2] PM	Source[3] PM	Other names
HII0530	56.27201	23.702707	20.3	-44.5	1.0	1.0	1.0	0.97	D, T: T	HII530 HD23326 Tr163
HII0531	56.27723	24.263523	20.0	-45.0	1.1	1.0	1.0	0.97	?, T: T	HII531 HD23325 Tr162
HII0627	56.350533	24.885977	19.9	-43.8	1.2	1.2	1.0	0.96	?, T: T	HII627 HD23352 Tr187
HII0636	56.34248	23.471731	16.26	-39.34	0.23	0.23	1.0	0.93	D, ?: D	HII636 Tr190 DH390
HII0652	56.358902	24.03514	18.1	-45.1	1.0	1.0	1.0	0.95	D, T: T	HII652 HD23361 Tr195
HII0676	56.373203	23.760529	15.2	-41.75	0.16	0.16	1.0	0.89	D, ?: D	HII676 Tr203 HCG190 DH395
HII0686	56.387222	24.303242	15.33	-38.89	0.43	0.43	1.0	0.91	D, ?: D	HII686 Tr206 HCG192
HII0708	56.397484	24.08321	21.81	-37.44	0.8	0.8	1.0	0.2	D, ?: D	HII708 Tr213
HII0740	56.426872	25.05709	10.21	-34.36	0.88	0.87	0.95	0.12	D, ?: D	HII740
HII0746	56.424374	24.431513	19.73	-44.07	0.75	0.75	1.0	0.64	D, ?: D	HII746
HII0879	56.52706	24.56742	16.45	-43.22	0.48	0.48	1.0	0.86	D, ?: D	HII879 Tr253 DH420
HII0882	56.517178	23.405537	22.23	-37.87	1.04	1.03	0.96	0.19	D, ?: D	HII882 Tr256 DH418
HII0883	56.528744	24.562807	16.73	-42.06	0.6	0.6	1.0	0.91	D, ?: D	HII883 Tr257 HCG208
HII0916	56.54894	24.622314	14.79	-51.74	0.46	0.46	1.0	0.09	D, ?: D	HII916 Tr268 DH428
HII0923	56.541874	23.340015	22.0	-51.8	0.9	0.9	0.9	0.72	D, T: T	HII923 Tr270 DH427
HII0974	56.58531	24.78548	13.42	-42.07	1.18	1.19	1.0	0.73	D, ?: D	HII974 Tr284 SK475 DH438
HII0996	56.59448	24.570177	10.21	-53.29	1.89	1.89	1.0	0.03	D, ?: D	HII996 HD282963 Tr289
HII1005	56.60015	24.361542	15.5	-38.77	0.46	0.46	1.0	0.91	D, ?: D	
HII1015	56.613968	25.135563	20.0	-44.6	1.4	1.4	1.0	0.97	?, T: T	HII1015 HD282952 TrR13 DH448
HII1032	56.618378	24.433918	21.9	-40.29	1.23	1.23	1.0	0.34	D, ?: D	HII1032 Tr296 DH450
HII1095	56.65739	24.747698	13.32	-57.38	1.52	1.54	1.0	0.01	D, ?: D	HII1095 Tr316 DH462
HII1110	56.662018	24.520338	16.94	-41.49	0.4	0.4	1.0	0.93	D, ?: D	HII1110 Tr322
HII1122	56.663857	24.103243	13.54	-51.28	1.34	1.33	1.0	0.11	D, ?: D	HII1122 HD23511 Tr327
HII1124	56.664104	24.029688	16.57	-40.21	0.26	0.26	1.0	0.94	D, ?: D	HII1124 Tr329 DH463
HII1132	56.659985	22.919804	21.1	-43.0	1.1	1.0	1.0	0.94	D, T: T	HII1132 HD23514
HII1139	56.666656	23.11037	17.2	-46.5	1.2	1.2	1.0	0.91	D, T: T	HII1139 HD23513 Tr331
HII1182	56.696087	22.914593	19.8	-46.6	1.4	1.4	1.0	0.96	D, T: T	HII1182
HII1200	56.71057	23.239195	17.6	-37.9	1.0	1.0	0.94	0.22	D, T: T	HII1200 Tr346
HII1207	56.72883	24.796349	17.7	-45.8	1.8	1.8	0.98	0.93	D, T: T	HII1207 HD282962 Tr348 DH477
HII1215	56.72391	23.5836	20.2	-43.9	1.6	1.7	0.99	0.95	D, T: T	HII1215 Tr350
HII1220	56.72192	22.880943	16.47	-43.54	0.5	0.5	1.0	0.84	D, ?: D	HII1220
HII1284	56.76755	23.995174	19.3	-44.4	1.1	1.0	1.0	0.97	D, T: T	HII1284 HD23585 Tr365
HII1298	56.77825	23.71517	10.02	-41.36	0.29	0.29	1.0	0.25	D, ?: D	HII1298 Tr369
HII1305	56.78061	23.22634	16.64	-41.2	0.18	0.18	1.0	0.93	D, ?: D	HII1305 HCG255 DH493
HII1309	56.791893	24.276672	20.4	-44.6	1.1	1.1	1.0	0.97	D, T: T	HII1309 HD23584 Tr372
HII1332	56.806374	23.71431	14.35	-40.36	0.32	0.32	1.0	0.87	D, ?: D	HII1332 Tr378
HII1362	56.830624	24.139126	19.2	-43.0	1.2	1.1	1.0	0.94	D, T: T	HII1362 HD23607 Tr390
HII1407	56.845417	22.922121	20.9	-47.9	1.1	1.0	1.0	0.93	?, T: T	HII1407 HD23610 TrS108
HII1454	56.89032	24.684223	14.87	-42.39	0.54	0.54	1.0	0.83	D, ?: D	HII1454 HCG278 DH521
HII1514	56.918537	24.364594	12.97	-40.48	0.62	0.62	1.0	0.69	D, ?: D	HII1514 HD282967 Tr430
HII1531	56.922657	23.971945	17.64	-38.44	0.35	0.35	1.0	0.85	D, ?: D	HII1531 Tr435 HCG285 DH532
HII1532	56.92158	23.740294	17.03	-39.34	0.33	0.33	0.99	0.92	D, ?: D	HII1532 HCG286 SK405 B270
HII1593	56.950462	23.21814	19.0	-45.2	2.3	2.4	0.95	0.94	D, T: T	HII1593 Tr444
HII1613	56.968838	23.941282	16.15	-51.94	0.94	0.94	1.0	0.09	D, ?: D	HII1613 HD282973 Tr448

Table 2. continued.

Name	RA (deg)	DEC (deg)	pmRA (arcsec)	pmDEC (arcsec)	epmRA (arcsec)	epmDE (arcsec)	Prob[1] All	Prob[2] PM	Source[3] PM	Other names
HII1756	57.045776	23.507023	17.87	-38.56	0.19	0.19	0.99	0.84	D, ?: D	HII1756 SK378 DH557
HII1776	57.07372	25.047886	10.68	-56.07	1.32	1.32	1.0	0.01	D, ?: D	HII1776 Tr495 DH567
HII1794	57.071342	23.890385	11.52	-44.12	1.26	1.26	1.0	0.34	D, ?: D	HII1794 HD282972 Tr499
HII1797	57.070457	23.636806	21.06	-30.59	1.65	1.65	1.0	0.05	D, ?: D	HII1797 Tr500
HII1856	57.109024	24.048445	21.32	-44.71	0.83	0.82	1.0	0.32	D, ?: D	HII1856 HD282971 Tr514
HII1883	57.116787	23.300774	21.45	-41.83	0.31	0.31	1.0	0.33	D, ?: D	HII1883 Tr520 HCG331 DH579
HII1924	57.143806	23.434818	14.06	-39.77	1.43	1.43	1.0	0.84	D, ?: D	HII1924
HII2016	57.189312	23.338873	10.47	-42.09	1.13	1.13	0.97	0.3	D, ?: D	HII2016 Tr557 HCG344
HII2034	57.20551	23.97732	15.98	-37.61	0.4	0.4	1.0	0.86	D, ?: D	HII2034 Tr563 HCG348
HII2106	57.24369	23.20123	15.9	-38.91	0.72	0.71	1.0	0.91	D, ?: D	HII2106
HII2126	57.259705	23.252468	12.77	-39.06	1.43	1.41	1.0	0.72	D, ?: D	HII2126 Tr584
HII2244	57.335793	24.77667	13.38	-55.0	5.6	5.6	0.99	0.2	D, ?: D	HII2244 Tr616 HCG369 DH613
HII2284	57.350216	23.839287	14.24	-44.01	1.16	1.16	1.0	0.65	D, ?: D	HII2284 Tr628
HII2311	57.369747	23.712238	15.89	-41.04	0.44	0.44	1.0	0.93	D, ?: D	HII2311
HII2341	57.388004	23.795427	18.18	-36.44	1.32	1.32	1.0	0.61	D, ?: D	HII2341 Tr649
HII2345	57.38634	23.380413	19.7	-43.6	0.9	0.8	1.0	0.97	D, T: T	HII2345 HD23912 Tr651
HII2366	57.402245	24.296135	13.75	-40.82	0.89	0.89	1.0	0.81	D, ?: D	HII2366 Tr657
HII2415	57.420506	23.341612	19.6	-43.8	0.9	0.9	1.0	0.97	D, T: T	HII2415 HD23924 Tr670
HII2462	57.459827	23.705631	14.86	-40.87	0.44	0.44	1.0	0.9	D, ?: D	HII2462 Tr680
HII2506	57.485363	23.218641	18.5	-43.8	1.1	1.1	0.99	0.95	D, T: T	HII2506
HII2588	57.551674	24.532957	15.81	-42.09	0.4	0.4	1.0	0.9	D, ?: D	HII2588 HCG387 Tr712 DH658
HII2644	57.58708	24.466755	16.39	-42.25	1.15	1.15	1.0	0.89	D, ?: D	HII2644 Tr727
HII2665	57.588753	23.096392	20.6	-44.1	1.7	1.9	0.99	0.95	D, T: T	HII2665
HII2741	57.64405	24.507822	18.22	-39.72	0.19	0.19	1.0	0.87	D, ?: D	HII2741 DH675
HII2786	57.666985	23.933065	16.05	-45.84	0.75	0.76	1.0	0.51	D, ?: D	HII2786 HD283067 Tr772
HII2870	57.714333	23.3291	14.87	-42.37	0.2	0.2	1.0	0.83	D, ?: D	HII2870 DH685
HII2880	57.729527	24.197466	9.71	-38.92	1.02	1.02	1.0	0.22	D, ?: D	HII2880 Tr795
HII2927	57.77326	24.736776	14.56	-40.14	0.3	0.3	1.0	0.89	D, ?: D	HII2927 HCG418 DH693
HII3019	57.851673	24.087425	16.79	-41.54	0.15	0.15	1.0	0.93	D, ?: D	HII3019 HCG429 DH710
HII3031	57.86342	24.518692	22.4	-44.7	1.2	1.1	0.99	0.93	D, T: T	HII3031 HD24132 Tr848
HII3063	57.874737	23.899223	22.52	-44.44	0.16	0.16	0.92	0.16	D, ?: D	HII3063 Tr862 HCG431 DH713
HII3096	57.91365	24.54894	22.75	-42.07	0.47	0.47	1.0	0.18	D, ?: D	HII3096 Tr879 DH721
HII3163	57.972446	24.387018	15.15	-29.05	1.23	1.23	0.86	0.04	D, ?: D	HII3163 Tr911 HCG444 DH725
HII3179	57.98689	23.901966	20.3	-47.1	1.2	1.3	1.0	0.96	D, T: T	HII3179 HD24194 TrR21
HII3187	57.988895	23.33944	17.89	-41.16	0.23	0.23	0.98	0.91	D, ?: D	HII3187 DH730
mhodb3	55.475456	23.084862	17.73	-41.19	0.21	0.21	1.0	0.92	D, ?: D	DH174

[1] Membership probability based on proper motion and photometry.
[2] Membership probability based on proper motion only (Sarro et al. 2014).
[3] Proper motions from: “D” = DANCe (Bouy et al. 2013), “T” = Tycho (Høg et al. 2000), and final selection.

Table 3. Several stellar properties, including lithium, rotation and activity data for the Pleades lithium sample. Only single stars with membership probability larger than 0.75, after removing binaries and suspected binaries.

Name	WLi[1]	eWLi	Ref	WLi[2]	eWLi	Ref	Temp		L_{bol}	eL_{bol}	ALi	eALi	eALi	Prot	eProt	Amp	Vsini	Ref	Rot	Li	Log Lx	eLx
	(mÅ)	(mÅ)		(mÅ)	(mÅ)		(K)[3]	(K)[4]	($L_\odot$)	($L_\odot$)		(1σ)	(3σ)	(d)	(d)	(mag)	(km/s)		type	type	(erg/s)	(erg/s)
AK I-1-317	78	10	Ma07	78	10	Ma07	6250	6305	1.95	1.8E-1	2.973	0.029	0.085	–	–	–	60.0	Ma07	–		–	–
AK II-437	142	10	Ma07	142	10	Ma07	6250	6304	1.60	1.4E-1	3.406	0.025	0.074	–	–	–	29.3	Qu98	–		–	–
AK III-756	120	10	Ma07	120	10	Ma07	6000	5987	1.50	1.3E-1	2.993	0.026	0.077	1.63715883	2.9E-5	0.0079	36.2	Qu98	A		–	–
BPL163	≤70	–	Da15	≤70	–	Da15	2800	2755	0.00169	1.9E-4	≤0.353	–	–	–	–	–	–	–	–		–	–
BPL327	≤200	–	Da15	≤200	–	Da15	2700	2681	0.00128	1.4E-4	≤1.166	–	–	–	–	–	–	–	–		–	–
CFHT-PL-11	500	–	St98	500	–	St98	2700	2711	0.0013	1.3E-4	2.769	0.015	0.032	–	–	–	–	–	–		–	–
CFHT-PL-12	800	–	St98	800	–	St98	2600	2586	0.00183	2.1E-4	3.334	0.015	0.034	–	–	–	–	–	–		–	–
CFHT-PL-16	1200	–	Mt00	1200	–	Mt00	2500	2501	0.00118	1.4E-4	3.567	0.015	0.035	–	–	–	–	–	–		–	–
Calar-03	1800	400	Re96	41800	400	Re96	2600	2558	0.00076	9.0E-5	3.567	0.014	0.033	–	–	–	–	–	–		–	–
LZJ-50	≤70	–	Da15	≤70	–	Da15	2800	2744	0.00174	1.9E-4	≤0.353	–	–	–	–	–	–	–	–		–	–
MHObd33	800::	–	St98	800::	–	St98	2500	2557	0.00129	1.4E-4	3.334	0.015	0.034	–	–	–	–	–	–		–	–
PPL-14	350	90	Da15	350	90	Da15	2700	2706	0.00153	1.7E-4	2.183	0.165	0.498	–	–	–	–	–	–		–	–
PPl-15	500	100	Ba96	1500	100	Ba96	2600	2628	0.00168	1.9E-4	2.769	0.048	0.144	–	–	–	–	–	–		–	–
Pels124	98	10	Ma07	98	10	Ma07	6250	6372	1.73	1.5E-1	3.172	0.028	0.079	–	–	–	20.5	Qu98	–		–	–
Pels192	80	15	So93	80	15	So93	4000	3988	0.0840	7.3E-3	0.43	0.038	0.107	–	–	–	10.0	So93b	–		–	–
Roque13	2500	–	St98	2500	–	St98	2600	2581	0.0011	1.3E-4	3.567	0.014	0.033	–	–	–	–	–	–		–	–
Teide01	1000	200	Re96	1000	200	Re96	2500	2536	0.00068	9.0E-5	3.567	0.036	0.135	–	–	–	–	–	–		–	–
Teide02	770	150	Mt98	1770	150	St98	2700	2723	0.00135	1.6E-4	3.292	0.07	0.216	–	–	–	–	–	–		–	–
hcg0332	900	90	Op97	900	90	Op97	3000	2904	0.0290	2.7E-3	3.461	0.036	0.107	–	–	–	58.0	Op97	–		–	–
hii0025	81	10	Ma07	57	15	So93	6500	6481	2.43	2.3E-1	2.931	0.048	0.148	–	–	–	44.2	Qu98	–		29.09	0.232
hii0034	166	10	Ma07	134	15	So93	5000	5075	0.331	3.1E-2	2.118	0.035	0.103	6.65058293	1.4E-3	0.0197	5.9	Qu98	S		29.05	0.162
hii0097[Bin?]	74	10	Ma07	75	5	Jo96	4500	4586	0.230	2.2E-2	1.106	0.027	0.077	6.74947635	9.6E-4	0.0354	6.8	Qu98	S		29.46	0.092
hii0120	152	15	So93	152	15	So93	5500	5683	0.765	7.0E-2	2.899	0.034	0.101	3.99034976	7.2E-4	0.0217	9.4	Qu98	S		–	–
hii0129	176	15	So93	176	15	So93	5250	5253	0.510	4.6E-2	2.573	0.035	0.104	5.34002688	1.0E-3	0.0181	5.3	Qu98	S		–	–
hii0133	55	20	Jo96	55	5	Jo96	4100	4194	0.0835	7.8E-3	0.422	0.023	0.068	1.3569575	2.3E-5	0.078	16.0	Te00	F		29.50	0.115
hii0152	191.2	10	Ki10	191.2	10	Ki10	5750	5767	0.829	7.6E-2	3.233	0.027	0.08	3.887814	4.2E-4	0.0332	11.8	Qu98	S		–	–
hii0158	36	10	Ma07	36	10	Ma07	7500	7535	6.30	5.6E-1	2.72	0.04	0.127	–	–	–	33.0	Ma07	–		–	–
hii0164	67	10	Ma07	59	15	So93	6500	6405	2.39	2.2E-1	2.889	0.048	0.144	–	–	–	38.9	Qu98	–		29.54	0.328
hii0174	301	10	Ma07	241	15	So93	5000	4997	0.446	4.1E-2	2.672	0.041	0.121	0.47429706	1.7E-6	0.0645	28.0	So93b	F	+	30.26	0.023
hii0193	161.5	10	Ki10	161.5	10	Ki10	5250	5265	0.538	4.9E-2	2.506	0.027	0.078	5.38756421	1.3E-3	0.0257	6.8	Qu98	S		29.9	0.232
hii0250[Bin?]	166.7	10	Ki10	166.7	10	Ki10	5750	5655	0.867	8.0E-2	2.96	0.027	0.078	4.23218914	1.0E-3	0.011	5.9	Qu98	S		29.46	0.092
hii0253	205	10	Ma07	186	15	So93	5500	5465	0.853	7.3E-2	2.878	0.036	0.104	1.47610499	7.0E-5	0.0259	38.2	Qu98	F		30.53	0.023
hii0263[Bin?]	252.1	10	Ki10	252.1	10	Ki10	5000	5007	0.444	4.1E-2	2.761	0.032	0.092	4.76537832	1.4E-5	0.0989	7.8	Qu98	A	+	29.87	0.069
hii0293	125	15	So93	125	15	So93	5500	5565	0.785	7.7E-2	2.617	0.034	0.103	3.92988991	2.2E-3	0.0153	5.1	Qu98	S		29.203	0.092
hii0324[Bin?]	202	10	Ma07	210	20	Jo96	4400	4389	0.164	1.6E-2	1.639	0.046	0.137	0.41188955	6.6E-7	0.1306	73.0	So93b	F	+	29.924	0.046
hii0344	26	10	Ma07	26	10	Ma07	7500	7554	6.70	6.1E-1	2.577	0.061	0.177	–	–	–	160.0	Ma07	–		–	–
hii0345	271	10	Ma07	245	15	So93	5000	4959	0.492	4.5E-2	2.647	0.04	0.12	0.84290118	3.5E-6	0.0231	18.9	Qu98	F	+	30.233	0.023
hii0380	200	10	Ma07	191	15	So93	4400	4343	0.138	1.3E-2	1.463	0.036	0.107	9.03288129	1.0E-8	0.0859	6.0	Qu98	S	+	–	–
hii0405	84	10	Ma07	81	15	So93	6250	6194	1.80	1.7E-1	2.905	0.04	0.119	1.92127951	1.5E-4	0.0253	18.2	Qu98	A		29.723	0.069
hii0430	140	10	Ma07	150	15	So93	5250	5365	0.485	4.5E-2	2.55	0.035	0.104	5.51856881	8.9E-4	0.0205	6.3	Qu98	S		28.8	0.351
hii0470[Bin?]	83	10	Ma07	62	15	So93	7000	7048	3.76	3.4E-1	2.99	0.044	0.136	–	–	–	<40.0	So93b	–		–	–
hii0489	140	10	Ma07	127	15	So93	5750	5851	1.068	9.7E-2	2.91	0.035	0.102	2.85024983	4.6E-4	0.0165	18.3	Qu98	A		29.393	0.115
hii0514	135	15	So93	135	15	So93	5750	5679	0.879	8.5E-2	2.794	0.036	0.102	3.79041574	1.5E-5	0.0236	10.5	Qu98	S		29.283	0.162
hii0530[Bin?]	76	10	Ma07	61	15	So93	7000	6918	3.59	3.2E-1	2.981	0.044	0.139	–	–	–	<12.0	So93b	–		–	–
hii0531	63	10	Ma07	63	10	Ma07	7250	7139	4.97	4.4E-1	2.897	0.034	0.1	–	–	–	75.5	Ma07	–		29.273	0.185
hii0627	108	10	Ma07	83	15	So93	6500	6413	2.08	1.8E-1	3.095	0.039	0.116	–	–	–	33.2	Qu98	–		29.563	0.069
hii0636	152	15	So93	152	15	So93	4750	4779	0.252	2.4E-2	1.847	0.035	0.103	7.5025171	1.5E-4	0.0154	3.5	Qu98	S		29.35	0.6
hii0652	21	10	Ma07	21	10	Ma07	7750	7669	7.52	6.7E-1	2.475	0.076	0.24	–	–	–	186.0	Ma07	–		–	–
hii0676	34	5	Jo96	34	5	Jo96	4200	4190	0.123	1.2E-2	0.19	0.028	0.082	7.0922232	2.9E-5	0.0211	5.5	Qu98	S		–	–
hii0686	150	20	Jo96	150	20	Jo96	4200	4149	0.125	1.1E-2	1.012	0.041	0.124	0.39763669	7.4E-7	0.1238	64.0	So93b	F	+	29.823	0.046
hii0708	97	10	Ma07	84	15	So93	6000	5882	1.50	1.4E-1	2.654	0.039	0.117	0.294			46.0	So93b	F		29.853	0.046
hii0740	152	10	Ma07	152	10	Ma07	4500	4498	0.118	1.1E-2	1.501	0.029	0.084	2.77192235	1.3E-4	0.1106	14.0	St87	A	+	–	–

Table 3. continued.

Name	WLi[1]	eWLi	Ref	WLi[2]	eWLi	Ref	Temp		L_{bol}	eL_{bol}	ALi	eALi	eALi	Prot	eProt	Amp	Vsini	Ref	Rot	Li	Log Lx	eLx
	(mÅ)	(mÅ)		(mÅ)	(mÅ)		(K)[3]	(K)[4]	($L_\odot$)	($L_\odot$)		(1σ)	(3σ)	(d)	(d)	(mag)	(km/s)		type	type	(erg/s)	(erg/s)
hii0746	107.6	10	Ki10	107.6	10	Ki10	5500	5465	0.558	5.1E-2	2.405	0.029	0.082	5.23230299	6.2E-4	0.0163	4.8	Qu98	S		29.133	0.139
hii0879	127	10	Ma07	152	15	So93	4500	4676	0.180	1.8E-2	1.705	0.037	0.104	7.064627	8.6E-4	0.0495	5.6	Qu98	S		28.98	0.179
hii0882	212	15	So93	212	15	So93	4500	4497	0.213	1.9E-2	1.795	0.038	0.109	0.57988155	2.5E-6	0.097	65.0	So93b	F	+	29.67	0.074
hii0883	50	10	Ma07	45	15	So93	4500	4532	0.153	1.5E-2	0.769	0.056	0.172	7.03724472	3.6E-3	0.0453	3.8	Qu98	S		28.98	0.179
hii0916[Bin?]	191.3	10	Ki10	191.3	10	Ki10	5000	5117	0.400	3.7E-2	2.499	0.028	0.083	5.91403628	1.0E-3	0.0539	5.6	Qu98	S		29.293	0.069
hii0923	171	10	Ma07	158	15	So93	6000	6051	1.41	1.3E-1	3.289	0.035	0.101	2.84578235	4.0E-4	0.0156	18.2	Qu98	A		29.55	0.094
hii0974	33	8	GL94	33	8	GL94	4200	4110	0.0972	9.2E-3	0.094	0.041	0.124	6.57829398	2.4E-5	0.0286	4.2	Qu98	S		29.003	0.28
hii0996	144	10	Ma07	132	15	So93	6000	5969	1.10	1.0E-1	3.052	0.035	0.103	3.08777064	2.8E-4	0.0188	11.9	Qu98	A		29.623	0.069
hii1005	46	10	Ma07	46	10	Ma07	4750	4908	0.176	1.5E-2	1.221	0.041	0.123	–	–	–	–	–	–		–	–
hii1015	145	15	So93	145	15	So93	6000	5887	1.014	8.8E-2	3.057	0.033	0.1	1.72095653	2.6E-5	0.0092	9.6	Qu98	A		29.403	0.115
hii1032	236	10	Ma07	212	15	So93	5250	5309	0.634	5.7E-2	2.864	0.038	0.113	1.32333028	1.1E-5	0.0417	37.2	Qu98	F	+	30.233	0.023
hii1095	154	10	Ma07	138	15	So93	5000	5099	0.350	3.4E-2	2.17	0.036	0.102	0.86705307	5.2E-5	0.0044	3.6	Qu98	F		29.073	0.328
hii1110	44	10	Ma07	21	15	So93	4400	4424	0.133	1.2E-2	0.265	0.117	0.4	7.96319798	3.2E-3	0.0274	5.9	Qu98	S		29.099	0.0
hii1122[Bin?]	85	10	Ma07	67	15	So93	6500	6622	2.69	2.6E-1	3.035	0.044	0.128	–	–	–	28.6	Qu98	–		29.623	0.069
hii1124	203	10	Ma07	217	15	So93	4750	4875	0.254	2.4E-2	2.349	0.038	0.113	6.41558	9.0E-5	0.0164	3.5	Qu98	S	+	29.543	0.069
hii1132	49	10	Ma07	46	15	So93	6500	6449	2.53	2.4E-1	2.792	0.056	0.16	–	–	–	40.0	So93b	–		–	–
hii1139	66	10	Ma07	51	15	So93	6500	6600	2.54	2.4E-1	2.887	0.052	0.151	–	–	–	31.4	Qu98	–		–	–
hii1182[Bin?]	156	10	Ma07	136	15	So93	6000	5879	1.055	9.8E-2	2.993	0.035	0.104	2.99605468	1.2E-4	0.0204	16.4	Qu98	A		–	–
hii1200	79	10	Ma07	67	15	So93	6250	6207	1.69	1.6E-1	2.802	0.046	0.136	–	–	–	13.7	Qu98	–		–	–
hii1207	141	15	So93	141	15	So93	6000	5977	1.05	1.0E-1	3.117	0.035	0.103	–	–	–	5.1	Qu98	–		–	–
hii1215	125	15	So93	125	15	So93	6000	5975	1.001	9.1E-2	3.014	0.035	0.103	–	–	–	4.1	Qu98	–		29.411	0.232
hii1220	158	15	So93	158	15	So93	5250	5289	0.371	3.3E-2	2.512	0.035	0.103	6.15460725	7.7E-4	0.0208	6.3	Qu98	S		–	–
hii1284	48	10	Ma07	48	10	Ma07	7500	7427	5.83	5.2E-1	2.843	0.036	0.106	–	–	–	107.5	Ma07	–		27.79	0.385
hii1298[Bin?]	98	10	Ma07	91	15	So93	4750	4846	0.261	2.5E-2	1.569	0.04	0.116	7.62860983	2.3E-3	0.0237	4.8	Qu98	S		29.58	0.092
hii1305	30	15	So93	≤60	–	Jo96	4300	4288	0.118	1.1E-2	≤0.577	–	–	0.3887814	8.2E-7	0.1049	84.0	So93b	F		29.37	0.175
hii1309	73	10	Ma07	42	15	So93	6500	6467	2.39	2.2E-1	2.762	0.057	0.182	–	–	–	85.0	So93b	–		29.67	0.046
hii1332	76	10	Ma07	35	15	So93	4750	4800	0.220	2.1E-2	1.013	0.069	0.213	8.17841955	5.3E-3	0.0213	5.3	Qu98	S		29.64	0.069
hii1362	28	10	Ma07	28	10	Ma07	7500	7592	5.96	5.4E-1	2.608	0.055	0.169	–	–	–	23.0	Ma07	–		–	–
hii1407	12	10	Ma07	12	10	Ma07	7750	7723	7.09	6.2E-1	2.207	0.14	0.575	–	–	–	25.0	Ma07	–		–	–
hii1454	158	10	Ma07	86	15	So93	4500	4669	0.175	1.7E-2	1.301	0.041	0.122	8.40559787	3.7E-5	0.0248	3.3	Qu98	S		29.233	0.28
hii1514	161	15	So93	161	15	So93	6000	5897	1.023	9.1E-2	3.163	0.036	0.102	3.25377982	3.2E-4	0.0284	13.6	Qu98	A		29.344	0.092
hii1531	65	10	Ma07	100	15	So93	4300	4216	0.122	1.1E-2	0.396	0.053	0.16	0.48300323	1.7E-6	0.0951	50.0	So93b	F		29.633	0.069
hii1532	48	10	Ma07	60	20	Jo96	4250	4308	0.0960	9.2E-3	0.604	0.063	0.187	0.78090716	5.4E-6	0.0685	50.0	So93b	F		29.502	0.115
hii1593	183.5	10	Ki10	183.5	10	Ki10	5500	5593	0.607	5.5E-2	3.001	0.027	0.079	5.05740707	5.7E-5	0.0077	1.8	Qu98	S		–	–
hii1613	120	10	Ma07	103	15	So93	6250	6316	1.69	1.6E-1	3.162	0.036	0.108	–	–	–	20.1	Qu98	–		29.377	0.115
hii1756	150	5	Jo96	150	5	Jo96	4000	3934	0.0843	7.9E-3	0.869	0.013	0.041	1.15276771	2.4E-4	0.034	5.0	Te00	F	+	28.88	0.282
hii1776	140	15	So93	140	15	So93	5500	5557	0.715	6.8E-2	2.7	0.035	0.101	4.49408203		0.037	9.8	Qu98	S		–	–
hii1794	84	10	Ma07	55	15	So93	6000	5995	1.11	1.0E-1	2.516	0.05	0.147	3.84662953	2.2E-6	0.0223	11.2	Qu98	S		29.01	0.128
hii1797	126	10	Ma07	125	15	So93	6250	6231	1.41	1.3E-1	3.238	0.035	0.106	–	–	–	19.6	Qu98	–		29.15	0.164
hii1856	105	10	Ma07	85	15	So93	6250	6161	1.52	1.4E-1	2.905	0.039	0.116	–	–	–	15.4	Qu98	–		29.173	0.162
hii1883	320	10	Ma07	250	20	Jo96	4500	4544	0.224	2.1E-2	2.101	0.05	0.147	0.23533495	2.1E-7	0.0585	140.0	So93b	F	+	29.71	0.6
hii1924	136	10	Ma07	141	15	So93	6000	6086	1.15	1.1E-1	3.213	0.035	0.101	2.89109736	6.1E-3	0.0173	14.2	Qu98	A		29.44	0.148
hii2016	148	15	So93	148	15	So93	4300	4375	0.121	1.1E-2	1.267	0.036	0.105	3.87950671	6.3E-4	0.0312	9.8	Qu98	A	+	–	–
hii2034[Bin?]	237	10	Ma07	222	15	So93	4500	4669	0.201	1.9E-2	2.099	0.039	0.116	0.55085229	2.4E-6	0.0579	75.0	So93b	F	+	29.743	0.046
hii2106[Bin?]	130	10	Ma07	116	15	So93	5000	5140	0.459	4.4E-2	2.09	0.036	0.108	3.04122134	4.0E-4	0.0135	8.0	Qu98	A		–	–
hii2126	184.9	10	Ki10	184.9	10	Ki10	5250	5302	0.395	3.8E-2	2.684	0.028	0.08	3.05658104	1.9E-4	0.0178	5.3	Qu98	A		–	–
hii2244	269	10	Ma07	268	15	So93	4500	4656	0.212	2.0E-2	2.388	0.043	0.124	0.56071931	3.2E-6	0.0394	50.0	So93b	F	+	30.063	0.046
hii2284[Bin?]	190.3	10	Ki10	190.3	10	Ki10	5250	5418	0.523	4.6E-2	2.85	0.028	0.083	5.81926006	2.3E-4	0.0109	3.7	Qu98	S		29.16	0.169
hii2311	170.4	10	Ki10	170.4	10	Ki10	5250	5438	0.500	4.8E-2	2.752	0.027	0.081	2.9331327	4.4E-4	0.0127	6.5	Qu98	A		28.82	0.317
hii2341	141	15	So93	141	15	So93	5750	5750	0.742	7.1E-2	2.904	0.035	0.103	4.88066973	3.3E-3	0.012	3.6	Qu98	S		29.09	0.201
hii2345	71	10	Ma07	38	15	So93	6750	6726	3.20	3.1E-1	2.743	0.059	0.185	–	–	–	130.0	So93b	–		29.76	0.312
hii2366	226.7	10	Ki10	226.7	10	Ki10	5250	5368	0.444	4.0E-2	3.032	0.031	0.088	6.21783952	1.3E-5	0.032	4.3	Qu98	S	+	28.923	0.115
hii2415	41	10	Ma07	41	10	Ma07	8000	8069	7.01	6.2E-1	2.788	0.037	0.112	–	–	–	30.5	Ma07	–		–	–

Table 3. continued.

Name	WLi[1]	eWLi	Ref	WLi[2]	eWLi	Ref	Temp		L_{bol}	eL_{bol}	ALi	eALi	eALi	Prot	eProt	Amp	Vsini	Ref	Rot	Li	Log Lx	eLx
	(mÅ)	(mÅ)		(mÅ)	(mÅ)		(K)[3]	(K)[4]	($L_\odot$)	($L_\odot$)		(1σ)	(3σ)	(d)	(d)	(mag)	(km/s)		type	type	(erg/s)	(erg/s)
hii2462	110.3	10	Ki10	110.3	10	Ki10	5250	5467	0.436	4.2E-2	2.425	0.028	0.082	6.92980587	2.4E-5	0.0216	4.9	Qu98	S		–	–
hii2506	128	10	Ma07	108	15	So93	6000	6005	1.23	1.2E-1	2.933	0.035	0.106	2.12103871	2.2E-4	0.0088	13.8	Qu98	A		–	–
hii2588	78	10	Ma07	78	15	So93	4400	4474	0.134	1.3E-2	0.973	0.043	0.129	5.97239848	1.4E-3	0.0453	5.2	Qu98	A		29.273	0.115
hii2644	186	15	So93	186	15	So93	5500	5594	0.619	5.9E-2	3.017	0.035	0.104	5.07153391	1.0E-8	0.0305	5.0	Qu98	S		29.113	0.162
hii2665	170	10	Ma07	166	15	So93	5250	5366	0.513	4.7E-2	2.645	0.035	0.104	5.38756421	2.4E-5	0.019	5.4	Qu98	S		–	–
hii2741	122	10	Ma07	91	15	So93	4750	4792	0.205	1.9E-2	1.501	0.04	0.115	5.15798051	2.3E-5	0.0469	7.8	Qu98	A		29.453	0.092
hii2786	146	10	Ma07	128	15	So93	6000	6071	1.19	1.1E-1	3.118	0.035	0.102	2.16659802	1.6E-4	0.0158	22.0	Qu98	A		29.453	0.139
hii2870	85	10	Ma07	69	15	So93	4750	4840	0.222	2.0E-2	1.402	0.046	0.134	7.89395278	2.4E-5	0.0422	4.0	Qu98	S		–	–
hii2880	142.3	10	Ki10	142.3	10	Ki10	5250	5261	0.400	3.4E-2	2.389	0.027	0.081	6.28238456	9.2E-4	0.0231	6.0	Qu98	S		29.053	0.185
hii2927	≤30	–	GL94	≤60	–	Jo96	4100	4046	0.0987	9.3E-3	≤0.316	–	–	0.26218183	2.9E-7	0.1174	95.0	So93b	F		29.413	0.162
hii3019	93	10	Ma07	51	15	So93	4300	4192	0.127	1.1E-2	0.381	0.052	0.156	5.46870223	4.3E-4	0.0446	6.0	Qu98	A		29.353	0.139
hii3031	63	10	Ma07	40	15	So93	7000	6935	3.98	3.5E-1	2.766	0.056	0.185	–	–	–	230.0	So93b	–		–	–
hii3063	135	10	Ma07	139	15	So93	4300	4292	0.122	1.2E-2	1.105	0.036	0.106	0.88393824	1.9E-5	0.0338	26.0	So93b	F	+	29.683	0.139
hii3096	254	10	Ma07	254	10	Ma07	5000	4987	0.295	2.8E-2	2.706	0.032	0.093	4.21255021	3.3E-4	0.1035	6.2	Qu98	A	+	29.813	0.069
hii3163	256	10	Ma07	222	15	So93	4500	4456	0.208	2.0E-2	1.801	0.038	0.113	0.41747738	8.6E-7	0.1092	60.0	So93b	F	+	29.853	0.069
hii3179[Bin?]	140.2	10	Ki10	140.2	10	Ki10	6000	6120	1.46	1.3E-1	3.238	0.025	0.074	4.85456989	9.3E-4	0.0077	4.3	Qu98	S		29.343	0.328
hii3187	93	10	Ma07	71	15	So93	4500	4464	0.153	1.4E-2	0.908	0.045	0.135	7.62860983	1.8E-5	0.0415	6.2	Qu98	S		–	–

Lithium and rotation sources: Ba96 = Basri et al. (1996), Da15 = Dahm (2015), GL94 = Garcia Lopez et al. (1994), Jo96 = Jones et al. (1996), Ki10 = King et al. (2010), Ma07 = Margheim (2007), Mt98 = Martin et al. (1998), Mt00 = Martín et al. (2000), Op97 = Oppenheimer et al. (1997), Qu98 = Queloz et al. (1998), Re96 = Rebolo et al. (1996), So93 = Soderblom et al. (1993b), So93b = Soderblom et al. (1993d), St98 = Stauffer et al. (1998a), Te00 = Terndrup et al. (2000), St87 = Stauffer & Hartmann (1987).

[1] W(Li) selection based primarily on the S/N.

[2] W(Li) selection based primarily on the spectral resolution.

[3] Effective temperature for the minimum χ^2 as derived with VOSA.

[4] Effective temperature after fitting Teff and χ^2 and minimizing this last value.

Bin? Suspected binary based on the spectra or the cross-correlation in Margheim (2007).